DEPARTMENT OF PHYSICS, UNIVERSITY OF JYVÄSKYLÄ
RESEARCH REPORT No. 4/1999

SPECTROSCOPY OF VERY NEUTRON DEFICIENT PO ISOTOPES UTILIZING THE RECOIL-DECAY TAGGING METHOD

BY
KERTTULI HELARIUTTA

Academic Dissertation
for the Degree of
Doctor of Philosophy

Jyväskylä, Finland
August 1999

URN:ISBN:978-951-39-9455-6
ISBN 978-951-39-9455-6 (PDF)
ISSN 0075-465X

Jyväskylän yliopisto, 2022

ISBN 951-39-0493-8
ISSN 0075-465X

DEPARTMENT OF PHYSICS, UNIVERSITY OF JYVÄSKYLÄ
RESEARCH REPORT No. 4/1999

SPECTROSCOPY OF VERY NEUTRON DEFICIENT PO ISOTOPES UTILIZING THE RECOIL-DECAY TAGGING METHOD

BY
KERTTULI HELARIUTTA

Academic Dissertation
for the Degree of
Doctor of Philosophy

To be presented, by permission of the
Faculty of Mathematics and Natural Sciences
of the University of Jyväskylä,
for public examination in Auditorium FYS 1 of the
University of Jyväskylä on October 1, 1999,
at 12 o'clock noon

Jyväskylä, Finland
August 1999

Kopi-Jyvä Oy
Jyväskylä 1999

Preface

This work has been carried out at the Accelerator Laboratory and the Department of Physics in the University of Jyväskylä during the years 1995-1999.

I would like to thank my supervisor Prof. Rauno Julin for his help, guidance and patience during my thesis work. His enthusiastic attitude towards γ-ray spectroscopy gave motivation to get over the moments of disbelief. I wish to express my gratitude also to Dr. Sakari Juutinen for teaching the secrets of the measurement electronics and data analysis, and to Prof. Matti Leino for guiding me into the world of α decay measurements. I am grateful to the past and present members of the RITU-γ group for creating an atmosphere where working was both easy and fun. Special thanks go to the "gamma-girls" for numerous and valuable discussions especially during the lunch breaks.

I want to thank the staff of the Department of Physics for the friendly and inspiring atmosphere. It has also been a great pleasure to make the acquaintance of the tens of scientists from different countries visiting our group during this work.

The financial support from the Graduate School in Particle and Nuclear Physics is gratefully acknowledged.

I am indebted to my friends, especially to Katja for sharing the experience of writing a thesis, and to the ones at Jyväskylän Ratsastuskoulu (Jyväskylä Riding School), for reminding me that there is a life outside of the lab, too. My family is acknowledged for always being supportive but also permanently astonished of my achievements. Finally, I would like to thank Jari for all his patience, support and understanding during these years.

Jyväskylä, August 1999

Kerttuli Helariutta

Abstract

In this thesis an experimental setup, consisting of a gas-filled recoil separator RITU and varying germanium detector arrays has been commissioned at the accelerator laboratory of the University of Jyväskylä. The relevant analysis methods, including recoil gating and the recoil-decay tagging (RDT) method are discussed. The setup, combined with the RDT method has proven to be a very powerful tool in the study of heavy, very neutron-deficient nuclei.

With this setup, prompt and delayed γ rays from the neutron-deficient nuclei $^{192\text{-}195}$Po have been studied. The excited states in ^{192}Po have been observed for the first time. New excited levels, including isomeric states in ^{192,194}Po and tentative unfavoured states in the odd-mass isotopes ^{193,195}Po, have been identified. The new data has been combined with the existing energy-level systematics. The new results have been used to test several nuclear models used in the description of the neutron-deficient Po isotopes. The data are in accordance with the scheme of the coexisting normal spherical and intruding oblate structures crossing each other in Po isotopes with $N \leq 114$.

TABLE OF CONTENTS

1. INTRODUCTION

Modern nuclear physics concentrates on probing the nuclear matter under extreme conditions – for example at high spin, at extreme neutron to proton ratios or at high temperature. Such experiments produce new data which is essential for testing existing theories and for creating the basis for new ones. One approach used in interpreting the experimental data is to try to get information on the systematical behavior of some nuclear property as a function of some variable. An example of this is the evolution of α-decay energies and half-lives as a function of the neutron number for a given element. The other perspective is to study some specific phenomenon that is characteristic of the behavior of nuclear matter in some special conditions. Such phenomena include superdeformation and shape coexistence in nuclei. In this work nuclear structure is studied experimentally by detecting γ rays emitted by a nucleus while it de-excites. Due to the high energy resolution of modern detectors ($\approx$ 1 keV), γ-ray detection provides detailed information on the γ-ray energies and the channels through which the de-excitation proceeds. This information can be applied in a straightforward manner in the interpretation of the shape and motion of the nucleus.

Recently, neutron deficient nuclei around the lead region of the nuclear chart have been studied actively. The reason for the interest is the variety of nuclear shapes observed for nuclei in this region. The proton number of lead nuclei is magic (Z=82), i.e. the proton shell is closed. Closed shell nuclei are usually considered to be spherical in their shape. However, when moving in the neutron shell away from the magic number 126 towards the midshell, other nuclear shapes begin to compete with the spherical shape. There is even evidence for three different coexisting shapes at low excitation energy in a lead isotope [All 98]. This shape-coexistence phenomenon has also been observed in nuclei with proton number less than 82, e.g. in mercury nuclei. The experimental data on the neutron deficient nuclei with $Z > 82$ are still not quite as extensive as on the lighter side, thus shape-coexistence in these nuclei is not yet fully confirmed. In this work the polonium nuclei having neutron numbers 108-111 have been studied. These nuclei lie on the very neutron deficient side of the nuclear chart, close to the proton drip line. The purpose of the study has been to

search for evidence for the possible coexistence of different shapes in these Z = 84 nuclei and to try to find out whether the valence proton particles and valence proton holes can be considered as equal when creating the different shapes.

The experimental studies of very exotic nuclei are difficult due to low production rates for the nuclei of interest and high production rate for unwanted nuclei formed in competing reactions. In the reactions used in this work the most prominent reaction channel is fission, covering over 90% of all the reaction channels. In in-beam γ-ray spectroscopy the γ rays are detected at the target position, almost immediately after formation of the nucleus. If the nucleus of interest is produced with a low cross section, most of the detected γ rays originate from other reaction products. In the extreme cases, like in this work, the interesting γ rays are totally obscured by the large amount of background γ radiation. Several methods based on the use of various ancillary detectors in connection with the γ-ray detectors have been developed in order to suppress of this unwanted background. Some of these detect α particles, protons and neutrons evaporated in the fusion-evaporation reactions, and thus allow selection of the reaction channel leading to the nucleus of interest (e.g. [Joh 93, Sav 98]). Others measure the total energy and multiplicity of the γ rays, and these can be used to select nuclei decaying via long γ-ray cascades (e.g. [Sle 90, Nol 86]). The third set of detection systems is based on the detection of the actual reaction product. This has been done for example by using a recoil filter detector (RFD) [Hee 93]. The RFD setup is used mainly to discriminate between fusion-evaporation residues and fission products.

Other powerful devices for the separation of fusion-evaporation products are the recoil separators. These devices are based on the use of magnetic or/and electric separation of interesting reaction products from the other products and the detection of the separated recoils at the focal plane of the separator. In most of these separators recoils with different mass-to-charge ratio (m/q) are also separated from each other. The flight time of the recoils through the separator is short (usually around a microsecond) and uniform, allowing the possibility to correlate the detected recoils with the prompt γ rays. Moreover, the separated recoils can be identified by using special types of detectors at the focal plane of the separator.

1.1 Recoil separators in γ-ray spectroscopy

The first setup utilising the combination of a recoil separator and prompt γ-ray detection system was reported in 1986 by Simon et al. [Sim 86]. An array consisting of 20 NaI detector elements was used to observe prompt γ radiation around the target position while the evaporation residues were separated using the velocity filter SHIP [Mün 79]. At the focal plane of SHIP there was a position sensitive detector telescope which provided information on the time-of-flight, energy loss and kinetic energy of the recoil along with the energy of any emitted α radioactivity. The data were processed using the principle of recoil decay tagging (RDT)[1]: the accepted γ rays had to be in a prompt coincidence with the detection of a recoil at the SHIP focal plane and the recoil was identified using its known α-decay characteristics.

The next stage in the development of the recoil separator and γ-ray detector setups was the combination of an array of Compton-suppressed (see Ch 2.2) Ge detectors and the Daresbury recoil separator [Lis 87]. The Daresbury recoil separator [Jam 88] consisted of two Wien filters and a bending magnet and the separated recoils were focussed according to their m/q. The recoil detection system consisted of two parts: first a thin transmission detector for providing the position information, then a split anode ionisation chamber for energy loss and total energy information. With the recoil velocity near 1 MeV/A the energy loss signal in the ionisation chamber depended somewhat on the Z of the nucleus. This made possible the identification of γ rays from a specific nucleus by requiring a prompt concidence with the mass- and Z-identified recoil and the γ rays. Later [Pau 95] the setup was updated to have the Eurogam array of 45 Ge detectors around the target position and a double sided Si strip detector for charged particle detection at the focal plane. In this setup the recoils were identified using their subsequent α decay, i.e. the RDT method as in the SHIP setup was used.

---

[1] The name for the method was taken into use by Eddie Paul from the University of Liverpool.

Meanwhile, in Argonne National Laboratory, a new Fragment Mass Analyser (FMA) [Dav 92] had been commissioned. Separation of the ions in the FMA is based on the use of two electric and one magnetic dipole field. The reaction products are dispersed on the focal plane according to their m/q. Several detection systems have been used to measure the properties of the separated particles. These include a multiwire proportional counter (MWPC) and a parallel plate avalanche counter (PPAC) for position and energy loss information and split anode ionisation chamber for energy loss and total energy measurement. A double-sided Si–strip detector (DSSD) has been in use for the detection of charged-particle decay of the recoils. The first in-beam γ-ray detection setup utilizing the FMA consisted of ten Compton-suppressed Ge detectors [Bax 93]. Later, in 1995, this setup was followed by the AYE-Ball array of nine large volume and ten small volume Compton suppressed Ge detectors [Blu 96]. In 1997 the small Ge-detector array was replaced by a large-scale device, Gammasphere, consisting of about 100 Compton-suppressed large-volume Ge detectors [Lee 90]. In all these setups the data analysis has been based on the selection of the γ rays in prompt coincidence with the recoils. The recoils have been identified either by using the position and energy loss information giving the m/q and Z of the nucleus or by using the DSSD detector and the RDT method.

Yet another γ-ray detection setup utilizing a recoil separator has been constructed in Laboratori Nazionali di Legnaro, Italy [Spo 95]. The setup consists of the recoil separator CAMEL and the γ-ray detector array GASP. The separation of recoils in the CAMEL recoil mass spectrometer is based on the use of two electric and one magnetic dipole unit like in the FMA at Argonne. The GASP array, holding a maximum of 40 Compton-suppressed Ge detectors and a BGO multiplicity filter detector, is positioned 4 meters upstream from the separator. Due to the large gap between the target and the separator, two additional quadrupole magnets have been installed in between the GASP array and the CAMEL separator for focussing of the recoils into the separator. The recoils are identified using their position on the focal plane, which is obtained from the position sensitive parallel plate avalanche counter (PS-PPAC), and their flight time through the separator.

1.2 Development of recoil gated γ-ray detection in Jyväskylä

The first tests combining a γ-ray detection system and the recoil separator RITU [Lei 95b] at the accelerator laboratory of the Department of Physics, University of Jyväskylä (JYFL), were performed in 1995. The test setup consisted of one Compton-suppressed Ge detector facing the RITU target chamber. Two reactions, ^{159}Tb(^{22}Ne,4n)^{177}Re and ^{141}Pr(^{40}Ar,4n)^{177}Ir, leading to previously well-known isotopes were used. Gamma-ray spectra in coincidence with any recoil detected by the RITU focal-plane detector were compared to the singles γ-ray spectra. An improvement in peak-to-background in the spectra of both test cases due to the recoil gating was observed [Uus 96].

Due to the encouraging results from the first test run, an array of nine Compton-suppressed TESSA-type [Nol 85] Ge detectors, DORIS, was set up in conjunction with RITU in spring of 1996. This combination was used in both recoil-decay tagging and in recoil gating modes (see Ch.3.3). With this setup the feasibility of the RDT method for studies of heavy neutron-deficient nuclei was demonstrated: the excited states of ^{194}Po, produced with the cross-section of about 200 μb, were observed with sufficient statistics to allow the analysis of γγ coincidences. After that, as a real breakthrough, the excited states in ^{192}Po were observed for the first time [Hel 96]. This was also the first time that in-beam γ-ray spectroscopy was performed on a nucleus produced with the cross-section of $\leq$ 10 μb.

In 1997 the DORIS array was replaced by the Jurosphere array which is able to accommodate ten TESSA type and 15 Eurogam phase I type [Bea 92] Compton-suppressed Ge detectors. This setup was used in 22 experiments and provided new data on the excited states of several neutron-deficient nuclei with Z ranging from 76 to 92 and with the lowest cross-section of 200 nb (^{198}Rn [Tay 99]).

After the Jurosphere, the next Ge detector system used with RITU was the SARI array built up from three segmented and one normal clover-type Ge detectors. This setup

was in operation during the spring and summer of 1998. The setup was used also with the inclusion of a detection system for prompt conversion electrons. The most recent γ-ray detector setup in connection with RITU is Jurosphere II, which began operation in spring 1999. It consists of 15 Eurogam phase I detectors, five Nordball-type detectors [Sle 90] and seven TESSA-type detectors around the target position. In these measurements a separate Ge detector array of three Nordball and two TESSA type detectors was constructed around the focal plane of RITU.

In this thesis, the combinations of different γ-ray detector systems with the RITU recoil separator will be discussed in detail. Basics of the methods used in the analysis of the data involving recoil-decay tagging are presented. Finally, results from the experiments focused on the studies of neutron-deficient polonium nuclei using this setup are shown and the underlying physics is discussed.

2. INSTRUMENTATION

2.1 Recoil separator

The idea of a recoil separator is to provide a fast method to separate nuclei of different masses using magnetic and electric fields. The nuclei are usually produced in the interaction of a high-energy accelerated ion beam with a target made of a suitable element. A common reaction used in the study of heavy elements is the fusion-evaporation reaction where the beam and the target nucleus fuse to form a highly excited compound nucleus. After the compound nucleus has evaporated a few nucleons and/or α particles the final nucleus is formed in its excited state. The separation of these evaporation residues passing through a magnetic recoil separator is defined by

$$\rho = \frac{mv}{qB}, \tag{2.1}$$

where the radius ρ of the track of a particle is given in terms of its velocity v, mass m, charge q and the magnetic field B where it moves. The velocity of the particle is assumed to be perpendicular to the magnetic field. In the fusion reaction the evaporation residues, i.e. the nuclei of interest, are ions having a narrow velocity distribution but a wide distribution of charges. According to (2.1) that results in a splitting of the radii of the tracks of elements having a single mass. In a recoil separator this means that the separated reaction products end up in a wide area at the focal plane of the separator (see figure 2.1 a)). That causes a problem in detecting the separated particles: either a very large detector has to be used or only a couple of charge states has to be selected. Because of practical reasons the latter alternative is usually chosen, although it results in a decreased detection efficiency of the wanted evaporation residues.

A means to avoid the problem caused by the wide charge distribution of the recoiling ions is to use a gas-filled recoil separator. The first gas-filled recoil separator was

built in the fifties at Oak Ridge National Laboratory and used in connection with a nuclear reactor for studying fission products [Coh 58]. Similar kinds of setups were also in use in Münich and Jülich from the sixties to the eighties. Later gas-filled separators have been employed in connection with accelerators in Dubna and Berkeley to separate fusion-evaporation residues produced in heavy-ion reactions from the primary beam and other reaction products, especially fission fragments. The idea in gas-filled separators is to fill the region of the magnetic field of the separator with a gas at a low pressure. When the ions pass through the gas they undergo several charge-exchange reactions. These reactions make the ions follow a trajectory that is determined by the average charge state of the ions so that all the particles, independent of their original ionic charge state end up in a relatively small area at the focal plane of the separator (see figure 2.1 b)). This results in a much enchanced transmission through the separator.

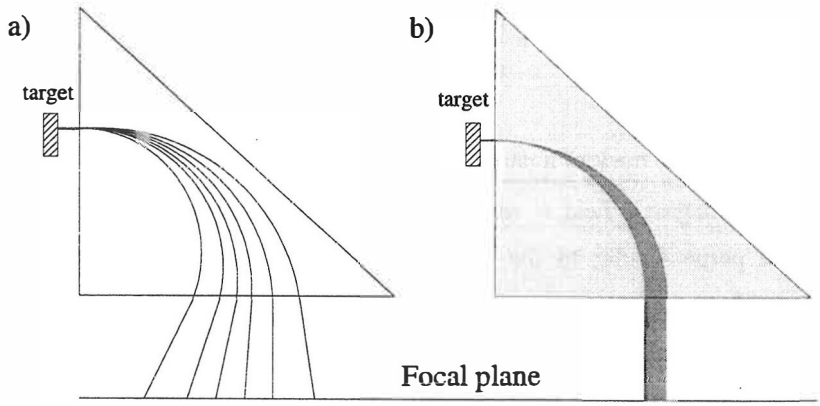

Figure 2.1. a) The tracks of the ions in a vacuum mode recoil separator. b) The tracks of the ions in a gas-filled recoil separator.

The average charge state of the ions travelling through low-pressure gas is determined by their velocity v [Boh 41]:

$$q_{ave} \approx \frac{v}{v_0} Z^{1/3}, \tag{2.2}$$

where v_0 is the Bohr velocity 2.19×10^6 m/s and Z is the atomic number of the ion. This q_{ave} is well defined in the velocity range of $1 < v/v_0 < Z^{2/3}$. In the experiments discussed in this thesis, the velocity of the recoiling fusion-evaporation residue is about 2% of the speed of the light and Z is close to 82. These values give $v/v_0 \approx 2.74$ which is much smaller than $Z^{2/3}$, thus the approximation of q_{ave} is valid.

Inserting (2.2) for the charge in (2.1) one gets

$$B\rho \approx \frac{mv_0}{Z^{1/3}} \approx 0.0227\frac{A}{Z^{1/3}} \quad [Tm], \tag{2.3}$$

where A is the mass number of the ion. From (2.3) one can see that the bending radius of the ion only depends on its atomic and mass numbers thus making the gas-filled recoil separator both a charge and velocity focussing device.

The Bρ resolution of the gas filled recoil separator depends on the gas pressure as shown in figure 2.2 [Arm 71]. An increase of the pressure enchances the charge exchange reaction and thus the resolution but at a certain limit the multiple scattering between the recoils and the filling gas starts to degrade the resolution. The other things affecting the resolution, besides the gas pressure, are the ion optical effects in the separator, the size of the recoil source and the velocity dispersion of the average charge [Ghi 88]. All these effects together form a range of gas pressures that gives the optimal resolution for the system. Still the Bρ resolution of the separator is low, typically of the order of 10 percent [Lei 95a]. For a reaction used in this work, ^{36}Ar + ^{160}Dy, the calculated ratio of magnetic rigidities of the fusion evaporation product ^{192}Po and the full energy beam particle is 1:0.31. This is enough to separate the primary beam from the wanted residues so that the full energy primary beam suppression at the focal plane is of the order of 10^{-12} to 10^{-15} [Ghi 88, Uus 96].

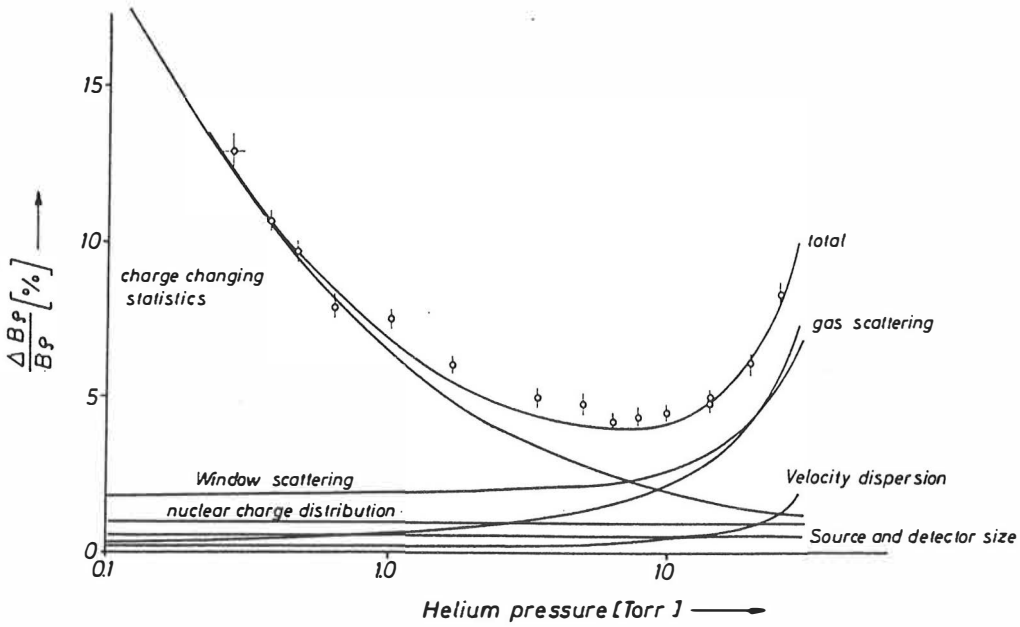

Figure 2.2. The dependence of the resolution of a gas-filled separator on the pressure [Arm 71].

2.1.1 Gas-filled separator RITU

The gas-filled recoil separator RITU [Lei 95b] (acronym for Recoil Ion Transport Unit) has been in operation in the accelerator laboratory JYFL since 1993. A drawing of the separator is shown in figure 2.7.

The magnetic configuration of RITU is QDQQ which means that in addition to the normal separator dipole and two focussing quadrupoles there is an additional vertically focussing quadrupole in front of the dipole magnet to get a better matching of the recoils to the dipole magnet acceptance. The filling gas of RITU is helium and the typical gas pressures are ranging from 0.5 to 3 mbar. To remove gaseous impurities from the separator, continuous helium gas flow is made use of. The whole helium volume is changed twice an hour. A thin carbon or nickel foil with a thickness ranging from 40-900 μg/cm2 is installed in front of RITU to separate the cyclotron and beam line vacuum from the helium filled separator chamber.

The focal plane detector of RITU is a 80 mm (hor.) x 35 mm (vert.) Si PIPS (Passivated Implanted Planar Silicon) detector, divided into 8 or 16 strips. Each strip is position sensitive in the vertical direction. The measured vertical position

resolution of the strip is better than 500 μm (FWHM) [Uus 96] so that the detector can be thought to be formed out of hundreds of small pixel detectors. The detector thickness is 300 μm. The ranges in Si for typical α particles are 20-50 μm and much less for the recoils (4-5 μm for polonium nuclei studied in this work). Therefore the detector is thick enough to stop the separated recoils and to detect their possible α decay. However, because the recoils get implanted quite close to the detector surface a part of the isotropically emitted α particles escape from the detector leaving just a part of their energy in the detector. The amount of escaping α particles is usually about 45%.

The Bρ resolution of RITU as all the gas-filled separators is limited. In practice this means that the recoils with a single Bρ value end up in a large spot at the focal plane. When the recoil distribution for a specific Bρ value is centered on the focal plane the distributions of other recoils with different Bρ values will partly overlap it. This is depicted in figure 2.3. which shows the horizontal recoil distributions on the RITU Si strip detector for two reaction products from the ^{36}Ar + ^{144}Sm fusion evaporation reaction. Due to the limited Bρ resolution it is not possible to identify the recoils by their m/q as in the vacuum mode separators. In RITU the recoils are identified by using correlated α-decay chains [Sch 79]. Correlated means that one or several α decays and a recoil implantation has to happen at the same position (or pixel) and the time between these events has to be within certain limits. The time limits are determined by the half-lives of the α decays. Using the known α-particle energies and half-lives that are characteristic to each isotope one can either identify the recoil ion or find new α emitters using the chain of several α decays.

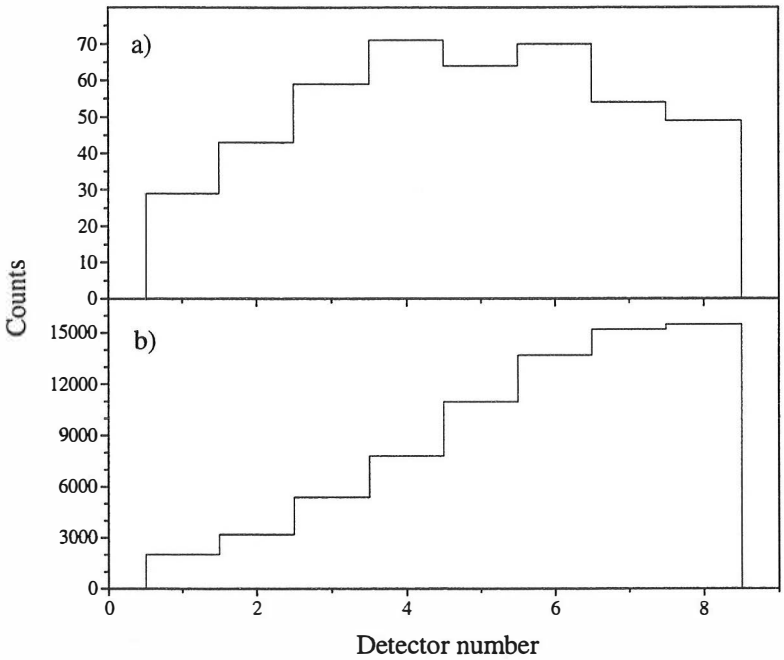

Figure 2.3. The horizontal distributions of two fusion evaporation products from the reaction $^{36}Ar + ^{144}Sm$. a) The recoil of interest, ^{176}Hg, and b) the side product, ^{176}Pt.

2.2 Gamma-ray detection system

When a nucleus is formed in a nuclear reaction it is in an excited state and it usually de-excites via prompt γ-ray emission within about 1 ns. During this time the reaction product moves only of the order of millimeters from the position it was created. This means that the detection system for the γ rays has to be around the target position. Some reaction products may de-excite via a longer living isomeric state. If the half-life of the isomeric state is of the order of the flight time through the recoil separator (≈ 1 μs) or longer, the nucleus may stay excited and emit γ rays after it has been implanted into the focal plane detector of the recoil separator. In this case a γ-ray detection system is needed also at the focal plane.

All the different γ-ray detection systems used in this work are based on the use of high purity Ge semiconductor detectors. The Ge detectors have a good energy resolution, FWHM usually 2-3 keV but because of the rather low Z of the Ge atoms (Z=32) the detection efficiency is limited. The efficiency of a Ge detector is usually given as a percentage of the efficiency of a 3x3 inch NaI(Tl) detector, measured with a ^{60}Co source (at 1.3 MeV) at a distance of 25 cm on the symmetry axis of the detector [Kan 95].

Gamma rays can have three different kinds of interactions with the Ge semiconductor crystal, photoelectric effect, Compton scattering and pair production. Photoelectric effect is dominant for the low-energy γ rays while pair production needs a γ-ray energy of at least 1022 keV ($2m_ec^2$). A full energy peak in the γ-ray spectrum is produced when the γ ray loses all of its energy in the interactions inside a detector crystal. Due to the relatively small Z and the finite size of the Ge crystal, a large number of the γ rays entering the detector escape again after Compton scattering and thus leave only a part of their energy in the crystal. This results in a continuum called Compton tail on the low-energy side of the full energy peak of the γ-ray spectrum.

To reduce the background caused by the Compton scattering an escape suppression shield (ESS) is installed around the Ge detector [Nol 85, Bea 92]. In the detectors used in this work the ESS units are made mainly out of bismuth germanate (BGO) which is a high-Z scintillator material and hence strongly absorbs γ rays. The ESS unit is used in anticoincidence with the Ge detector thus discarding γ rays scattered from the Ge crystal.

To increase the detection efficiency and to detect several γ rays emitted in a de-excitation of a nucleus at the same time, an array of several Ge detectors is needed. In this work, two different kinds of arrays consisting of several escape suppressed Ge detectors have been used. These arrays were installed around the target position to detect prompt γ rays. To detect delayed isomeric γ transitions at the focal plane a setup consisting of unsuppressed Ge detectors has been used.

2.2.1. DORIS array

The γ ray detection array DORIS was constructed from nine Compton suppressed TESSA type [Nol 85] Ge detectors. The relative efficiency of one TESSA detector is ~23% and the absolute photopeak efficiency for the whole array is about 0.5 % for the ^{60}Co 1332 keV γ rays. The detectors are packed in a compact dodecahedron geometry, the distances from the target to detectors range from 15 cm to 16.5 cm. The detector angles relative to the beam direction are 78°, 102° and 143°. At each angle there were three detectors.

A single TESSA type Compton suppressed Ge detector is presented in figure 2.4. A closed end coaxial cylindrical Ge crystal with a diameter of 52.3 mm and length of 56.8 mm is the main component of the detector. The suppression shield around the crystal is made out of BGO with NaI(Tl) front part. This is because the NaI(Tl) material has higher light output than BGO and can thus generate enough light to penetrate the layer of BGO and give a good signal to the photomultiplier tubes. In front of the suppression shield there is a lead collimator preventing γ rays from the target from directly hitting the suppression shield.

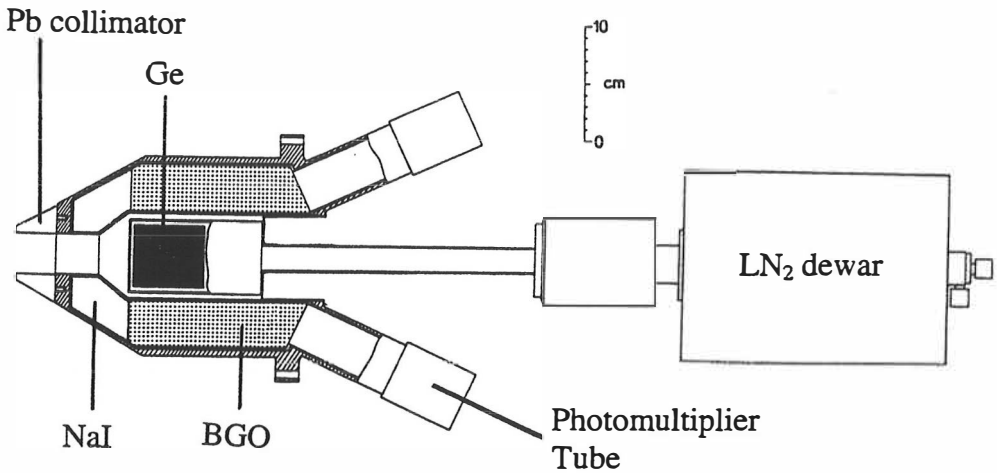

Figure 2.4. Escape suppressed TESSA type Ge detector [Nol 85].

A drawing of the DORIS array is shown in figure 2.5. The target chamber is a simple beam tube having an outer diameter of 38 mm. This enables a close geometry but complicates the practical use because the tube can accommodate only one target at a time. Changing of the target involves pressurizing and evacuation of the beam tube which is a slow process due to the sensitive beam window between the separator gas volume and the beam line vacuum.

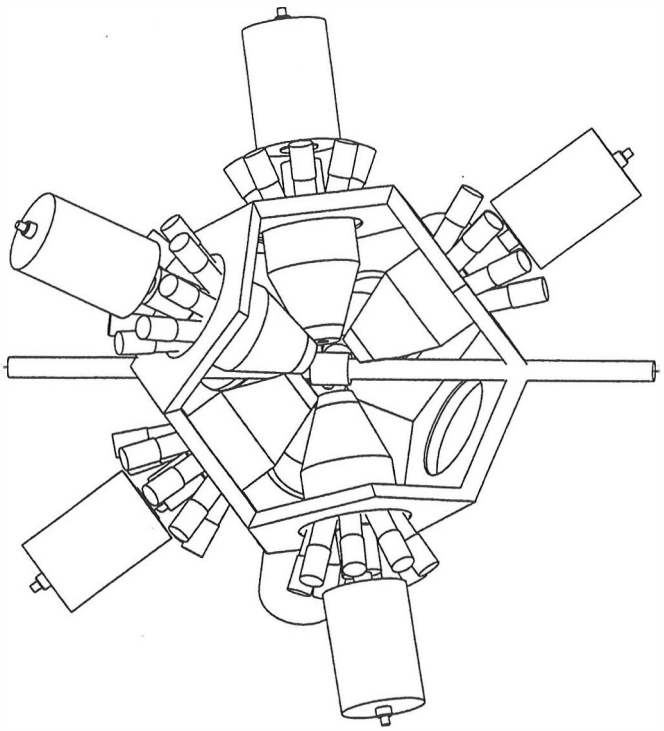

Figure 2.5. A schematic drawing of the DORIS array.

2.2.2 Jurosphere array

The Jurosphere array can accommodate 10 TESSA type detectors and 15 Eurogam phase I type detectors [Bea 92], all with the ESS units. The TESSA detectors are in two rings having angles of 79° and 101° relative to the beam direction. The Eurogam detectors are mounted into a Eurogam frame, ten at 134° and five at 158°. The relative efficiencies of the Eurogam detectors range from 65% to 85%. The diameter of the coaxial detector crystal is 69-75 mm and the length ≥ 70 mm. A drawing of a

Compton suppressed Eurogam detector is shown in figure 2.6. The BGO shield around the detector is thinner than that of the TESSA detector resulting in a slightly weaker Compton suppression.

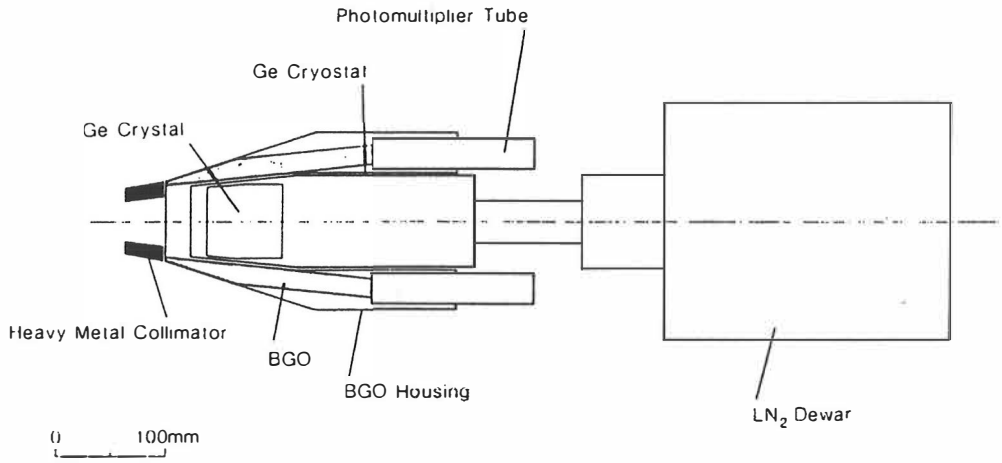

Figure 2.6. Escape suppressed Eurogam phase I Ge detector [Bea 92].

A schematic picture of the Jurosphere array connected to the RITU recoil separator is shown in figure 2.7. Depending on the availability of functioning detectors in the Jurosphere experiments the number of TESSA detectors ranged from 10 to 12 and the number of the Eurogam detectors from 9 to 14. With the different setups the absolute photopeak efficiency of the array for 1.3 MeV γ rays ranged from 1.2% to 1.7%.

In this setup the target chamber is half spherical, half cylindrical with a diameter of 10.5 cm (see fig. 2.8). The large target chamber renders it possible to use a target ladder system with several targets which simplifies the use of the setup compared to the DORIS setup. The distances of the detectors from the target were about 20 cm for both the TESSA and Eurogam detectors.

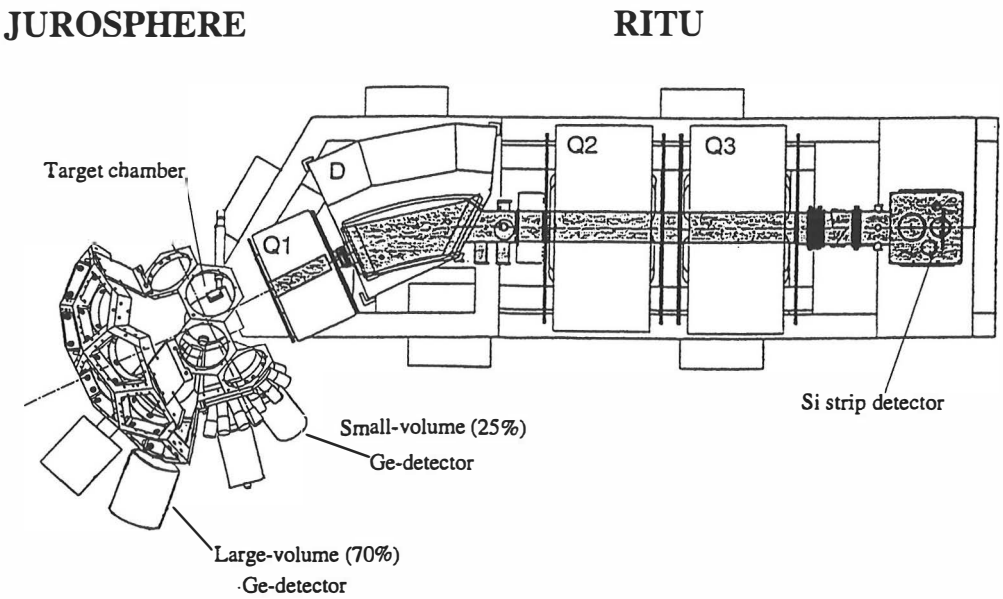

Figure 2.7. A schematic drawing of the Jurosphere-RITU setup. D and Q1-Q3 are the dipole magnet and the quadrupole magnets, respectively.

2.3 Combination of a recoil separator and a γ-ray detector array

2.3.1 Mechanical details

When combining a γ-ray detection system with a recoil separator the needs of both devices have to be taken into account. This is demonstrated in figure 2.8 where the beam line around the target position is presented for the RITU + Jurosphere setup. The construction of the target area in the DORIS + RITU setup was similar except for the target chamber (see Ch. 2.2.1).

The target (a) was positioned at a distance of 37 cm from the first quadrupole of RITU. At this distance it was still reasonably easy to fit in the Ge detector array without any significant loss of efficiency of RITU. The target was fixed onto a target ladder (b) that could accommodate 7 small (rectangle, 14 x 8 mm or 10 x 8 mm) or 5

big (round, diameter 15 mm) target frames. The target area could be separated from the beam line vacuum and RITU with two 100 mm valves (c). The gas filling of RITU extends to the gas window (d) so that the target lies in the gas volume. Carbon windows of 50-100 $\mu g/cm^2$ in thickness were used. To prevent the γ rays produced by the beam interacting with the gas window from reaching the Ge detectors a Pb shield (e) is installed around the beam tube downstream from the window. Upstream from the window there is an x-y slit system (f) consisting of four independently tuned tantalum plates. These slits can be used to cut the part of the beam which due to bad focussing could hit the window frame and cause additional γ-ray background. For connecting the different parts of the beam tube two bellows are utilized, one (g) before the gas window and the other (h) after the target chamber. The tube between the two bellows is fixed to the detector frame at point (i).

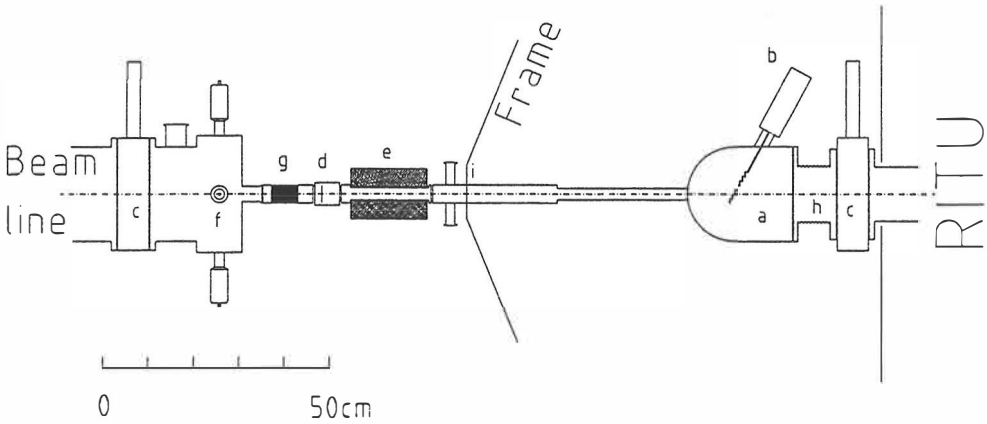

Figure 2.8. Beam line around the target position for the Jurosphere + RITU combination. See text for details.

2.3.2 The measurement electronics

The block diagram of the measurement electronics for the DORIS + RITU setup is shown in figure 2.9. The electronics for the Jurosphere + RITU setup was mainly similar to this. The RITU focal plane Si strip detector electronics has been discussed in detail in [Uus 96] and is not presented here. In the following the main principles of the signal processing and data acquisition are explained.

Single Ge detector

The general idea of the signal processing of all the Ge arrays in connection with RITU is the same. The preamplifiers of the Ge detectors have two similar outputs of which one is fed into a linear amplifier to produce a signal containing the energy information of the γ ray and the other is used for timing. A timing signal is also taken from the BGO shield detector. The timing signals are used for creating a gate signal that allows only γ-ray energies from the events fulfilling certain criteria to be recorded. The first criterium for an accepted γ ray is dictated by the escape suppression: the γ rays have to be in anticoincidence with any signal from the BGO shield. The second criterium prevents the pile-up of the signals caused by two γ rays entering the detector within a too short time interval compared to the time the amplifier needs to process a signal. The pile-up rejection is done in two ways. Firstly, the busy signal from the linear amplifier prevents the processing of another γ ray within the time the amplifier needs to process the first one. Secondly, if the time between the two pulses entering the amplifier is so short that the busy signal is not yet set the zero crossing point of the piled up bipolar output pulse of the amplifier is delayed. This distorted crossing time can be utilized to single out the piled-up signals from the clean single γ events.

Combination of several Ge detectors

The Ge timing signals from the first coincidence unit (* in fig 2.9) are fed into an OR unit (FAN) and a multiplicity unit (MLU) where fast Ge OR and AND signals are created, respectively. The width of the signal entering the units, 150 ns, limits the fast γ-γ coincidence window to about 300 ns. The output from the MLU unit is obtained if at least two γ rays are observed within this time window.

Signals from the Si strip detector

The position sensitivity of the RITU Si detector is achieved by dividing the detector horizontally into strips and using a resistive layer in each strip. The energy signal from the event in the detector is obtained by summing up the signals from the top and bottom ends of a strip. Due to the resistive layer the division of the signal to the top and bottom parts is proportional to the vertical position of the event. The two kinds of events happening in the RITU Si detector, the recoil implantation and the charged-particle decay, may differ quite a lot in energy. Therefore, in some cases two amplification channels are needed. The strip in which the event is taking place, i.e. the horizontal position of the event, is resolved by using a bit pattern unit. In addition to the energy and position signals a separate timing signal is extracted for every Si detector event.

Timing signals

Distributions of time differences between γ-ray events are generated by using time to amplitude converters (TAC) or time to digital converters (TDC). The TAC units are used for measuring the time between the γ-ray detection at the target position and the recoil implantation as well as the time between the first and the second γ ray in a $\gamma\gamma$ coincidence event. The TDC units are utilized when the time between a single γ-ray signal from each detector is measured with respect to the $\gamma\gamma$ coincidence signal. In addition to the relative time differences measured by the TAC and TDC units every event is stamped by an absolute clock signal. The clock runs with a frequency of 1 MHz and the time is represented by a 32 bit word. The clock thus cycles every 72 minutes.

Focal plane Ge detectors

In some setups an additional Ge detector (or several of them) is installed behind the focal plane strip detector to detect the delayed γ rays. In such a case an energy signal from an unsuppressed Ge detector and TAC based time signal between the recoil implantation and the focal plane γ-ray event are created. In the case of several Ge detectors at the focal plane also the time between different γ rays in an event is measured using a TAC unit.

Data acquisition

The data acquisition system consists of two parts: the acquisition electronics which is based on a set of VME crates with integrated electronics and the resource manager connected to a SUN workstation [Jon 95]. All the different signals are fed via analog to digital converters (ADC) to ADC interface cards. The data from the ADC cards are read out if a master trigger signal is present. This signal determines the type of data recorded – in figure 2.9 the master trigger requires either a signal from the Si detector or at least two signals from the Ge detectors to be present in an event. The events are read out to a high speed memory by a read out controller card. When the memory is filled, a Motorola Power PC processor unit reads out the data block and converts it into EUROGAM format [Cre 91]. After that the data block is transferred via a fiber distributed data interface (FDDI) card and optic fibre cable to the tapeserver that stores it onto Exabyte tape.

The acquisition is controlled by using the SUN workstation running the MIDAS data acquisition control system. This system makes possible also the viewing of the histograms that can be read out straight from the ADC cards. The workstation is also connected to the data stream going to the tapeserver in such a way that it allows the on-line sorting of the data using the EUROGAM type data sorting programs.

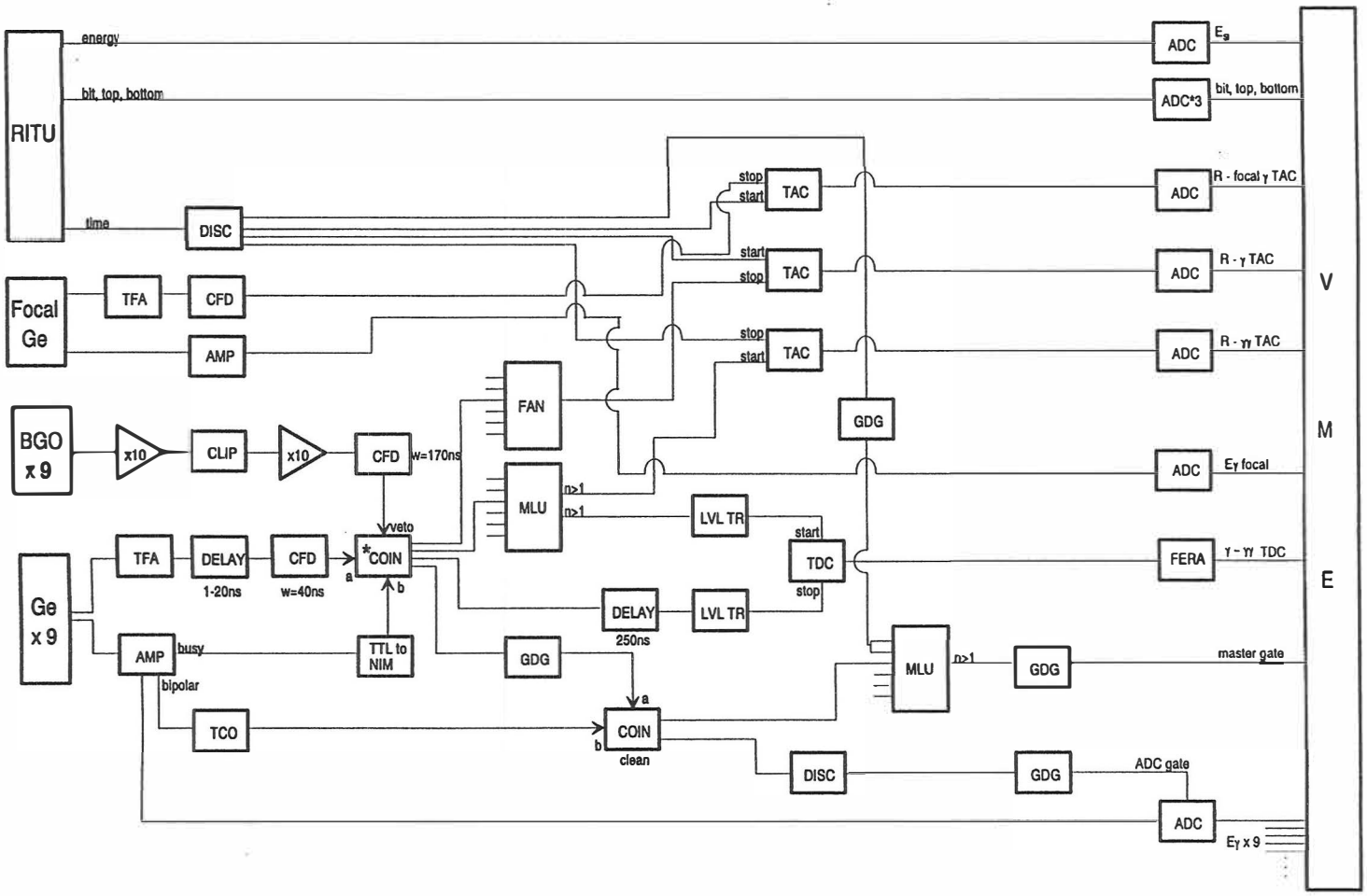

Figure 2.9. A block diagram of the electronics used in the DORIS + RITU setup.

2.4 Performance of the setup

2.4.1 General

In the experiments with the Jurosphere and DORIS arrays in conjunction with RITU heavy ion beams of ^{19}F, ^{22}Ne, $^{28,30}Si$, $^{36,40}Ar$, $^{40,42}Ca$, $^{58,60}Ni$, ^{63}Cu, ^{66}Zn and ^{74}Ge with kinetic energy ranging from 4.12 to 5.54 MeV per nucleon have been used. The targets have usually a thickness of about 500 $\mu g/cm^2$ to let the fusion-evaporation products fly away from the target and to minimize the energy loss and spread of the recoiling ions. The beam intensities have been about 10-20 particle nA. The beam intensity is limited either by the counting rate in the Ge detectors or in the focal plane Si strip detector, or by the durability of the target.

2.4.2 Transmission measurements

The combination of the Ge-detector array and RITU has been utilized to measure the transmission of RITU. The transmission of a separator refers to the percentage of certain reaction products transmitted from the target to the separator focal plane. However, the focal plane detector covers only a part of the focal plane and therefore not all the transmitted recoils are detected. The percentage of the recoils of certain species that are transmitted through the separator and observed by the focal plane detector is called the efficiency of the separator – detector system.

The transmission depends mainly on the design of the separator, i.e. the position of the target and the optimization of the geometry and the magnetic fields. In RITU the transmission is enhanced by the gas filling and by an additional quadrupole magnet installed in front of the dipole magnet. The optimal settings for the magnets are tuned individually for every experiment. In addition to the construction of the separator the transmission of a recoil separator is ruled by the properties of the separated recoil and the reaction in which it was formed. The transmission is enhanced in the symmetric reactions because the energy of the recoil is high and the recoil distribution strongly forward peaked. The distribution of recoils from a fusion-evaporation reaction is also determined by the nature of the evaporation channel. For example, pure neutron

evaporation from the compound nucleus results in a more narrow recoil distribution than the reactions involving an α particle evaporation.

To obtain the efficiency value for RITU the peak intensities of known γ-ray spectra from the plain Ge-detector array were compared with the peaks in a γ-ray spectrum where a coincidence with a recoil implantation was required. If the reaction products were well centered in the detector it was also possible to calculate the transmission value by assuming that the recoil distribution is Gaussian.

Figure 2.10 represents the γ (a) and recoil gated γ (b) spectra from the ^{28}Si (143 MeV) + ^{172}Yb $\rightarrow$ ^{200}Po* reaction. The spectra are gated by the 500 keV γ-ray transition in ^{196}Po. The intensities of the peaks at 464 keV, 429 keV, 584 keV, 238 keV and 254 keV were extracted for both of the spectra and the efficiency value of 18.3±0.2% was obtained as an weighted average of the five calculated efficiency values. The distribution of ^{196}Po recoils on the focal plane detector is shown in figure 2.10 c), together with the fitted Gaussian curve. From this figure it can be estimated that in this case 71±3% of the ^{196}Po recoils transmitted to the focal plane are detected. Using this value the transmission of 25.8±1.2% is obtained.

Efficiency and transmission values for different reactions and reaction products obtained by using the previously explained method are shown in table 2.1. If the centroid of the distribution of recoils of certain species is not within the focal plane detector only the efficiency value is given.

All the reactions in table 2.1 were rather asymmetric and the recoil velocities ranged from 1.5 to 2.2 percent of the speed of light. Clearly the nuclei produced through solely neutron evaporation had the highest transmission. According to the expectations the lowest transmission value was for the reaction involving evaporation of two alpha particles. The other cases with one alpha or proton emission lie in between these values.

Table 2.1. RITU efficiency and transmission values obtained using the recoil - γ coincidence technique.

Reaction	Evaporated particles	Recoil	Efficiency [%]	Transmission [%]
$^{36}Ar + ^{144}Sm$	2p2n	^{176}Pt	14.5 ± 0.3	- (*
$^{40}Ca + ^{148}Sm$	2α	^{180}Pt	5 ± 2	8 ± 3
$^{40}Ca + ^{148}Sm$	α2n	^{182}Hg	17 ± 5	23 ± 7
$^{40}Ca + ^{148}Sm$	αn	^{183}Hg	14 ± 3	22 ± 5
$^{40}Ca + ^{148}Sm$	2p2n	^{184}Hg	12 ± 4	17 ± 6
$^{28}Si + ^{171}Yb$	5n	^{194}Po	21 ± 2	28 ± 4
$^{28}Si + ^{172}Yb$	4n	^{196}Po	18.3 ± 0.2	25.8 ± 1.2
$^{40}Ar + ^{170}Er$	4n	^{206}Rn	23 ± 3	25 ± 3

(* the distribution is not centered, see fig. 2.3.

2.4.3 Background radiation

Background radiation detected by the Ge detectors increases the dead time of the signal-processing and data acquisition system and generates contamination peaks in the γ-ray spectra. In the Si strip detector background radiation increases the counting rate and thus random correlations when correlating α particles and recoils. Therefore it is very important to keep the level of background radiation in both the Ge and Si detectors as low as possible.

In addition to the unwanted reactions between the beam and the target, the background radiation detected by the Ge detectors is produced by the beam interactions with the He filling gas and the gas window. Unwanted radiation or background radiation is produced especially when the beam is scattered in the window and the gas and hits the target frame. These contributions can be determined in test runs by using empty target frames of different sizes, with or without gas window and with different gas pressures. The background radiation is reduced by minimizing the thickness of the gas window (40-100 $\mu g/cm^2$ C in this work) and the gas pressure, by using as big target frames as possible and by installing a lead shielding between the gas window and the Ge detectors. It has also been observed that significant background radiation is emitted by the reaction products created in the interaction of beam + ^{12}C gas window and implanted onto the walls of the target chamber.

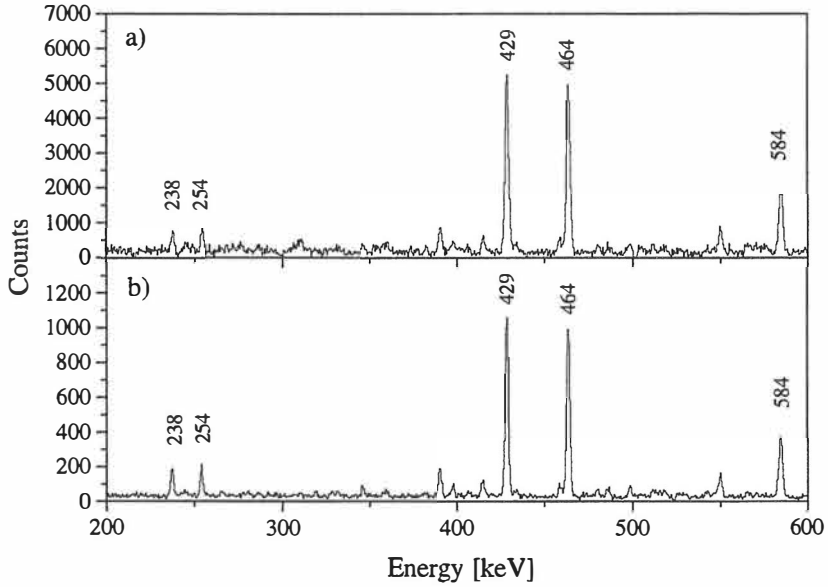

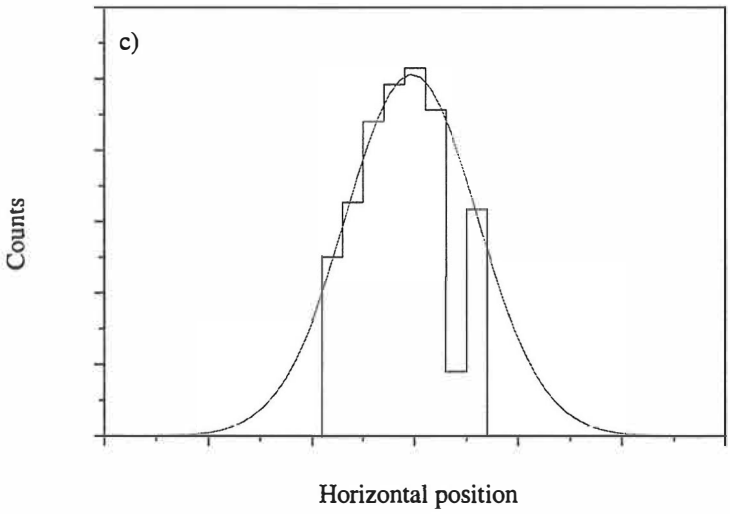

Figure 2.10. a) γ-ray spectrum from the ^{28}Si + ^{172}Yb reaction in coincidence with the ^{196}Po 500 keV transition. b) γ-ray spectrum from the ^{28}Si + ^{172}Yb reaction gated by the recoils observed at the focal plane detector of RITU and in coincidence with the ^{196}Po 500 keV transition. c) Distribution of the ^{196}Po recoils at the focal plane detector accompanied by a Gaussian curve fitted to the distribution.

Major background detected by the focal-plane Si-strip detector, especially in symmetric reactions, is due to the target knock-outs, target like transfer reaction products and scattered beam. This is because their $B\rho$ values are similar to those of the fusion products. The only possible ways to reduce this background are to change the gas pressure for optimizing the focus and to use an extended beam stopper after the dipole magnet. However, increasing of the gas pressure is often done at the expence of increasing γ-ray background. The use of the extended beam stopper decreases the transmission through RITU. All these effects make the optimization of the background conditions quite a complex task in the extreme cases.

In typical experiments with RITU and a Ge-detector array the major fusion-evaporation reaction product entering the Si detector is not the nucleus of interest. If the recoil of interest is produced in minor amounts compared to vast amounts of other fusion-evaporation products the α-recoil correlation analysis may be hindered. Fortunately when striving for the more and more exotic neutron deficient nuclei the α-decay half-lives get shorter which facilitates the correlation analysis. At the same time the α-decay energy of the nucleus of interest is usually the highest in the α spectrum and thus the α peak is easy to resolve and identify. In all experiments involving correlation analysis one should compare the counting rate in a Si detector pixel to the half-life of the nucleus of interest and this way try to estimate the maximum counting rate allowed in the Si detector.

3. DATA ANALYSIS

3.1 Data format

The data from the experiments are stored on magnetic Exabyte tapes using EUROGAM data format [Cre 91]. The data are saved on the tape in blocks, each block consisting of several events and ending in an end block token. An event starts with a start event token followed by several data words which include the output from different ADCs. Each data word contains an address and the actual data. An event consists of all the data read during the time the master trigger signal is on. The width of the master trigger signal is usually from 6 μs to 40 μs.

In the combined RITU and γ-ray detector setup the data words that may appear in an event are

- γ-ray energy
- γ-ray detection time relative to γγ coincidence signal (TDC)
- total energy of a recoil or an α-particle
- vertical position of a recoil or an α-particle (both from the top and the bottom of the detector)
- Si detector strip number (horizontal position)
- time between the detection of a γ-ray and a recoil or an α particle (TAC)
- time between the detection of the first and the second γ ray in a γγ event (TAC)
- clock word.

In the case where the energies of the implanted recoils are significantly higher than the α-particle energies two amplification channels are used for the Si strip detector signals. This results in an additional set of data words for the energy, top, bottom and strip number signals from the Si detector.

3.2 Calibrations

3.2.1 Germanium detectors

Gain matching, energy calibration

The energy calibration and gain matching between different detectors is done using a calibration γ-ray radiation source consisting of mixed ^{133}Ba and ^{152}Eu. This source emits γ rays of a wide energy range, from 80 keV to 1408 keV. This range was sufficient to give reliable calibrations for the γ-ray spectra obtained in the present experiments.

Because the prompt γ rays in the present experiments are emitted from forward-flying recoils the calibration obtained using the source has to be corrected due to the Doppler shifts. When a γ ray is emitted from a recoiling nucleus moving with a velocity v the energy of the γ ray is shifted to

$$E = E_0(1 + \frac{v}{c}\cos\theta) \tag{3.1}$$

where E_0 is the actual γ-ray transition energy and θ is the γ-ray emission angle relative to the recoil direction. In practice it is usually assumed that the recoil from a fusion-evaporation reaction flies in the beam direction even though the recoil velocity vectors have some angular distribution. In the reactions studied in this work this angular spread of the recoils causes a broadening of about 0.2% of the γ-ray energy for the γ peaks observed in the detectors at angles 78° and 102°. Additional Doppler broadening of similar magnitude results from the opening angle of the Ge detectors. Both of these broadening effects are reduced towards the backward angles as a function of $sin\theta$. The influence of these effects on the spectrum quality is small, especially in the Jurosphere array where most of the detection efficiency is in the backward angles.

Efficiency calibration

Due to the finite size of the Ge crystal the detection efficiency for γ rays changes as a function of the γ-ray energy. Efficiency calibration of the Ge detectors in the present work was based on the use of known γ-ray intensities from the ^{133}Ba and ^{152}Eu source.

Figure 3.1 shows the relative efficiency curve for the whole DORIS array. For small energies the detection efficiency is low. This is mainly due to the absorption of the γ rays in the special absorber plates utilised to reduce the high counting rate originating from the target X-rays. Due to the bad timing properties of the signals produced by the low-energy γ-rays the efficiency is cut also by the signal processing electronics. The maximum efficiency is reached at about 100 keV. After this the efficiency goes down as the probability of the photoelectric effect in the Ge crystal steeply decreases.

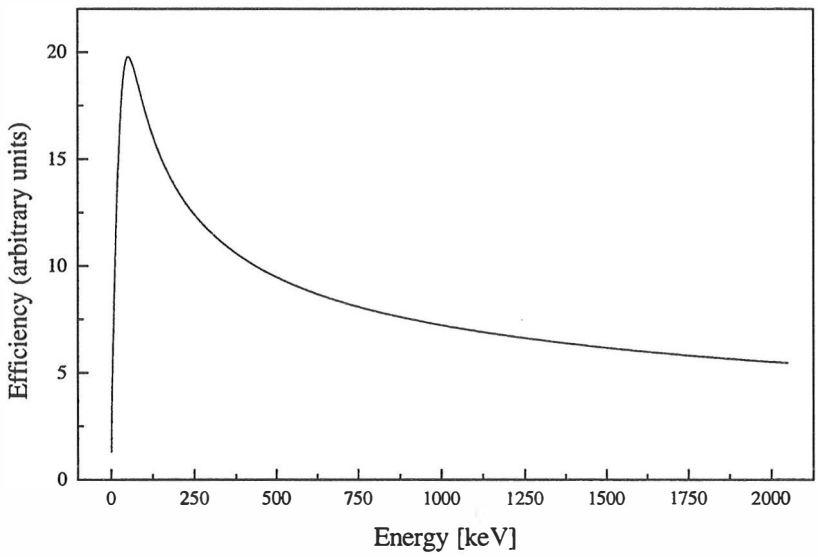

Figure 3.1. Efficiency curve for the whole DORIS array.

In addition to the relative detection efficiency the absolute detection efficiency of a Ge detector array is measured using the 1332 keV energy peak from a calibrated ^{60}Co source.

3.2.2 Silicon strip detector

Energy-position correction

The height of the energy signal from a single strip of the focal-plane Si detector depends on the position of the interaction. In figure 3.2 a) energies of α-particles emitted by fusion-evaporation residues from the reaction ^{36}Ar (178MeV) + ^{160}Dy ->

$^{196}Po^{*}$ have been plotted as a function of the α decay position, measured from the bottom of the detector. On the top of the figure a projection to the energy axis, i.e. the α-particle energy spectrum is shown. To enhance the resolution and in some cases, to even resolve the separate α peaks in the spectrum the position dependence of the α-particle energy has to be removed for all the strips. The result of such an energy-position correction is shown in figure 3.2 b) where the improvement in the α-particle energy resolution is clearly demonstrated.

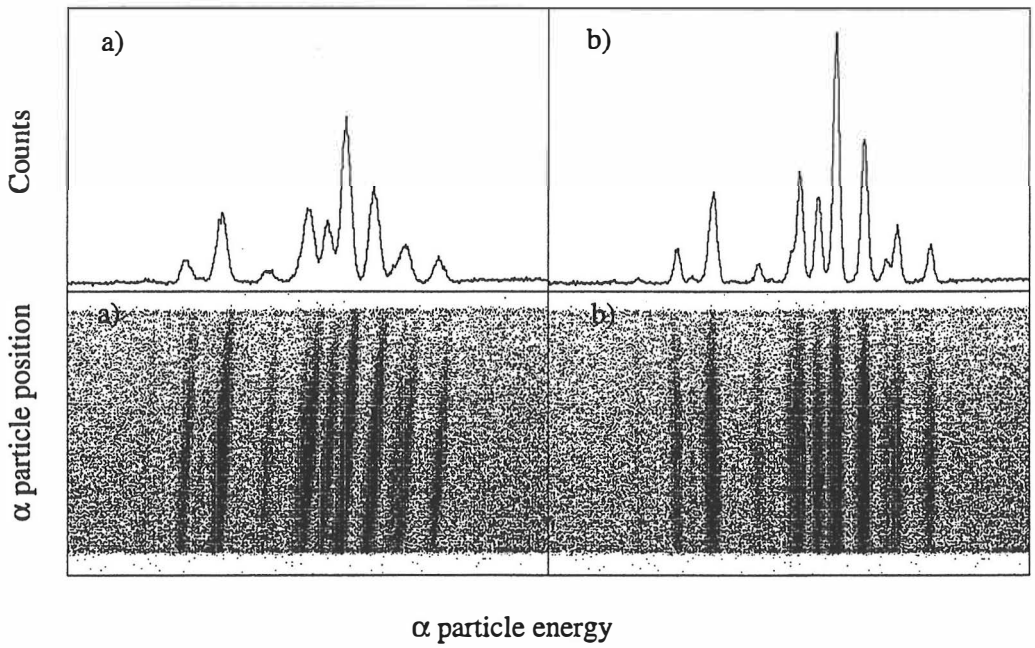

Figure 3.2. a) Dependence of the α-particle energy on the vertical position where the decay took place. On the top, the projection on the α-particle energy axis. b) The effect of removing the position dependence.

Gain matching, energy calibration

After the position dependence correction the α-particle energy spectra from the separate strips are gain matched and calibrated. In the recoil-decay tagging experiments the α decay properties of the recoil of interest and other major reaction products are normally known. Thus, the calibration is usually made internally, using the energies of the strong α peaks resulting from the α decays of known reaction products. Figure 3.3 shows a gain matched and calibrated total spectrum of α-particles emitted by the recoils from the reaction $^{36}Ar + ^{160}Dy \rightarrow ^{196}Po^{*}$.

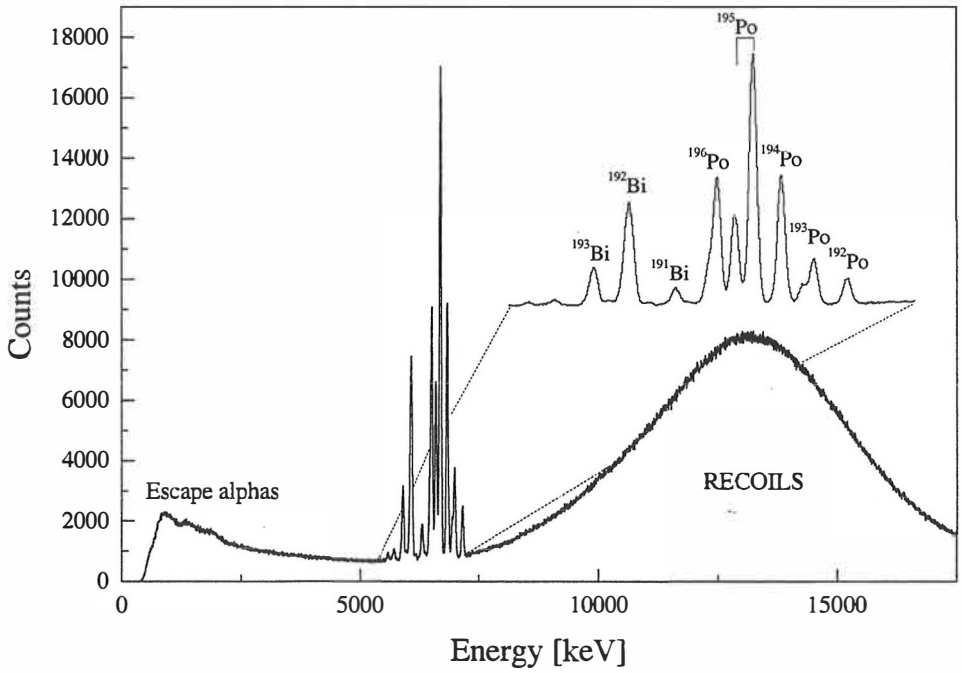

Figure 3.3. Total singles spectrum obtained from the Si focal plane detector from the reaction $^{36}Ar + ^{160}Dy \rightarrow ^{196}Po^{*}$. The part of the spectrum showing the α-particles emitted by the recoils is magnified.

Position-position calibration

When correlating a recoil implantation with a subsequent α decay one needs exact position information for both of the events. The processing of the recoil and the α events via different amplification channels results in position information that is

somewhat different for the separate channels. Therefore a relationship between the recoil position and the corresponding α position has to be determined.

In figure 3.4 the recoil position is plotted as a function of the position of subsequent short-lived α decay taken place in the same strip. The real correlations, i.e. the events where both the recoil and the α particle have been observed close to each other, are seen as a diagonal line. The more evenly distributed points represent the background resulting from the accidental correlations.

The detector is divided horizontally either to 8 or to 16 strips, giving a width of 10 mm or 5 mm, respectively, for a position bin in the horizontal direction. The vertical position from each strip is obtained as the ratio between the top or bottom signal and the sum energy signal. This ratio is multiplied by 1024 thus dividing the strip into 0.034 mm wide bins in Y direction. The α particles have a range of about 20-50 μm in the Si detector and the position signal itself does have a finite resolution. This implies that the recoil and the α particle do not have to be found exactly in the same bin to be correlated. The distribution of the distances between successive recoil implantations and α decays is shown in figure 3.5. The actual correlated events are seen as a peak on a background formed by the accidental recoil – α correlations. The shape of the random background is similar to the vertical recoil distribution. The position resolution in the vertical direction i.e. the FWHM of the peak in figure 3.5 is about 310 μm.

The effective number of pixels in the Si detector is determined by the counting rate in the detector as well as by the recoil distribution. Because the recoil distribution is strongly centered especially in the vertical direction the counting rate in the center of the detector is much higher than at the edges of the detector. This results in an increased probability of accidental correlations in the central detector area. Furthermore, this makes one position pixel in the central area seem to be larger than what is obtained by deriving the size of a pixel from the position resolution of the detector. Hence, the effective number of pixels in the Si detector is determined by the ratio between the rate of the recoil candidates implanted into the detector and the rate of the random correlations within the accepted position range. This number is found

to be in a normal case about 100 and 200 for a detector with 8 and 16 strips, respectively.

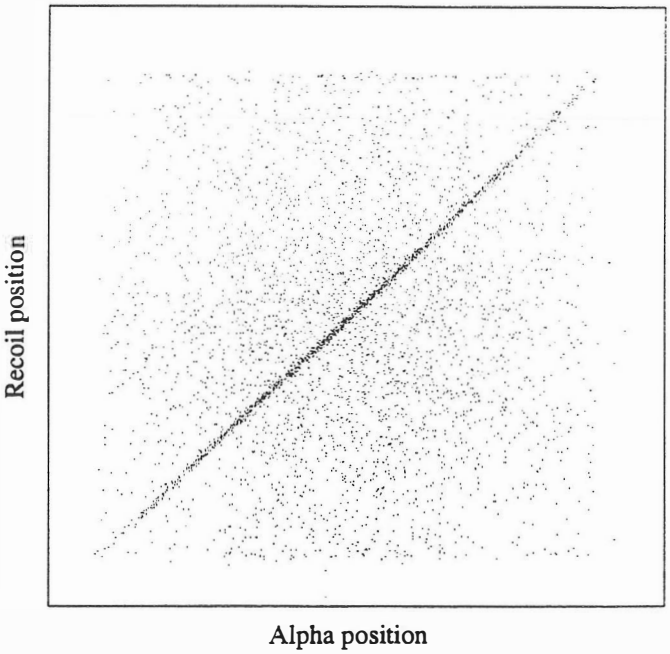

Figure 3.4. Positions of successive recoil and α events in one strip.

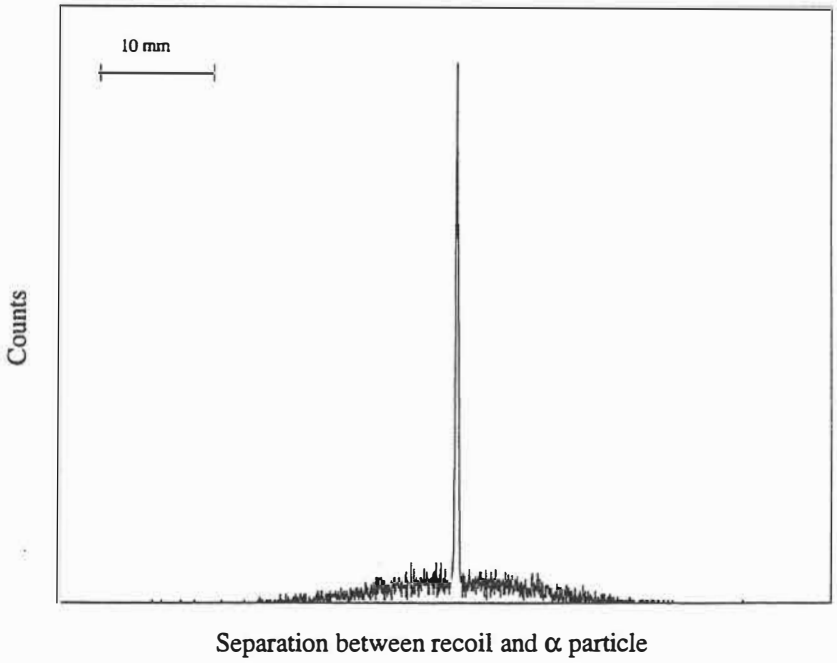

Figure 3.5. Position difference distribution for successive recoil and α events in one strip.

3.3 Analysis methods

3.3.1 Recoil gating

In the case where the nucleus of interest is one of the main fusion-evaporation products and the background from the target knockouts and scattered beam transported through the separator is small the recoil separator can be used simply as a trigger for γ-ray detection. In this mode all the γ rays occurring in prompt coincidence with the signal from the Si detector are accepted as good γ-ray events. In practice a prompt coincidence is identified by means of the recoil–γ TAC signal.

An example of a typical recoil-γ TAC spectrum generated by the DORIS + RITU setup from the reaction ^{36}Ar (178 MeV) + ^{160}Dy → ^{196}Po* is shown in figure 3.6. The spectrum consists of a peak formed by the prompt coincidences on the top of a flat background. A more detailed picture of the structure of this TAC spectrum is obtained by plotting it as a function of the energy from the Si strip detector, as shown in figure 3.7. In this experiment the α decay and recoil energies were similar and thus were processed via one amplification channel. The prompt recoil-γ events are seen in the plot as a banana-shaped concentration of points. The blurred upper edge of the area is formed by the low-energy γ-ray signals having poor timing properties. Above and below the prompt concentration there is a wave-like structure. This is produced by the TAC signals originating from random coincidences between the recoils and abundant target Coulomb excitation γ rays occurring during the cyclotron beam pulses. The random time distribution between the α particles and the γ rays is demonstrated by the vertical stripes across the spectrum.

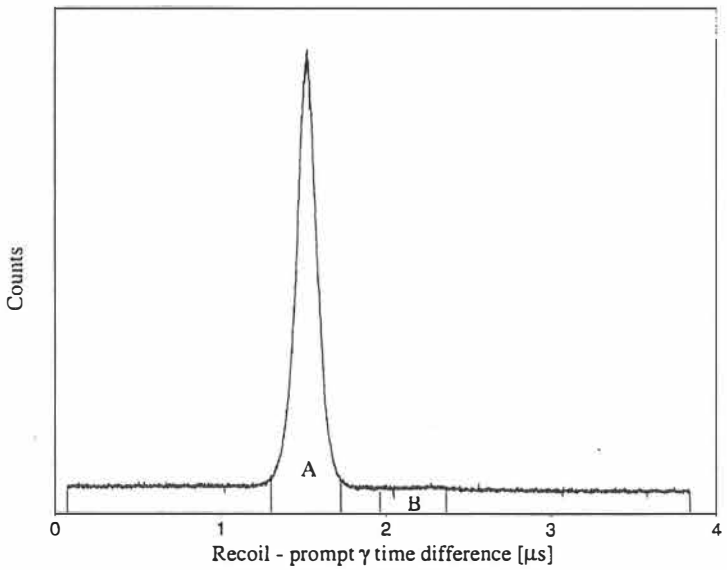

Figure 3.6. Recoil–γ TAC spectrum from the ^{36}Ar (178 MeV) + $^{160}Dy \rightarrow {}^{196}Po^{*}$ reaction. A and B are the gates used when creating the γ-ray spectrum.

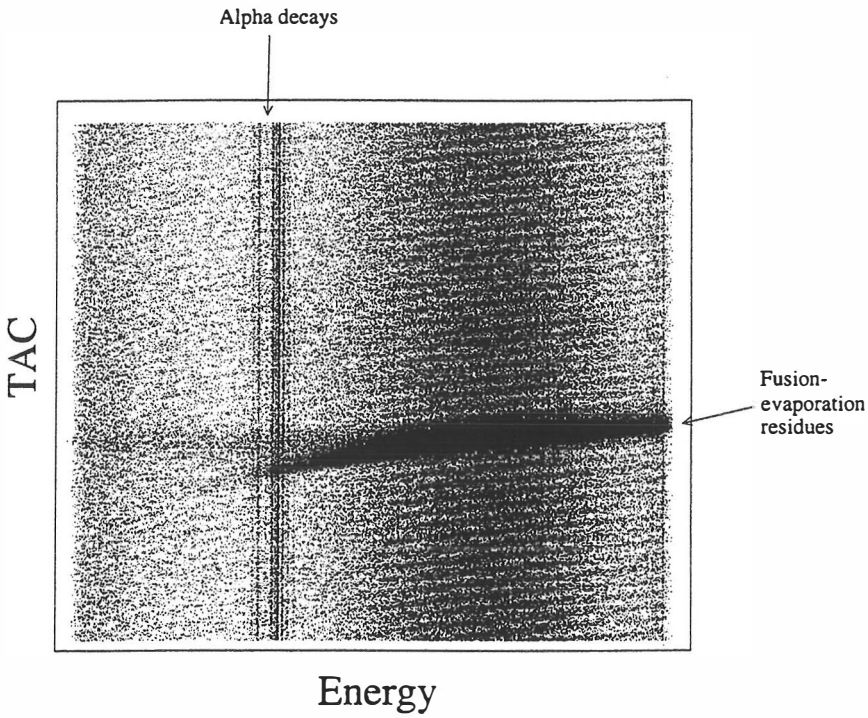

Figure 3.7. Recoil–γ TAC spectrum plotted as a function of the energy from the Si strip detector. See text for details.

A part of a γ-ray spectrum obtained by gating with the prompt peak (gate A, fig. 3.6) in the TAC spectrum of figure 3.6 is shown in figure 3.8 with thin line. In this spectrum γ- and X-rays from the fusion-evaporation residues (Po, Bi) are seen but also a remarkable amount of γ rays from Coulomb excitation and X-rays of the Dy target are present. These mainly random events originating from the flat background in the TAC spectrum are much reduced when the γ rays gated with a background gate (fig. 3.6, gate B) are subtracted from the spectrum, while the γ-ray peaks originating from the fusion-evaporation residues are unchanged. The result of this background subtraction is shown in figure 3.8 by the thick line.

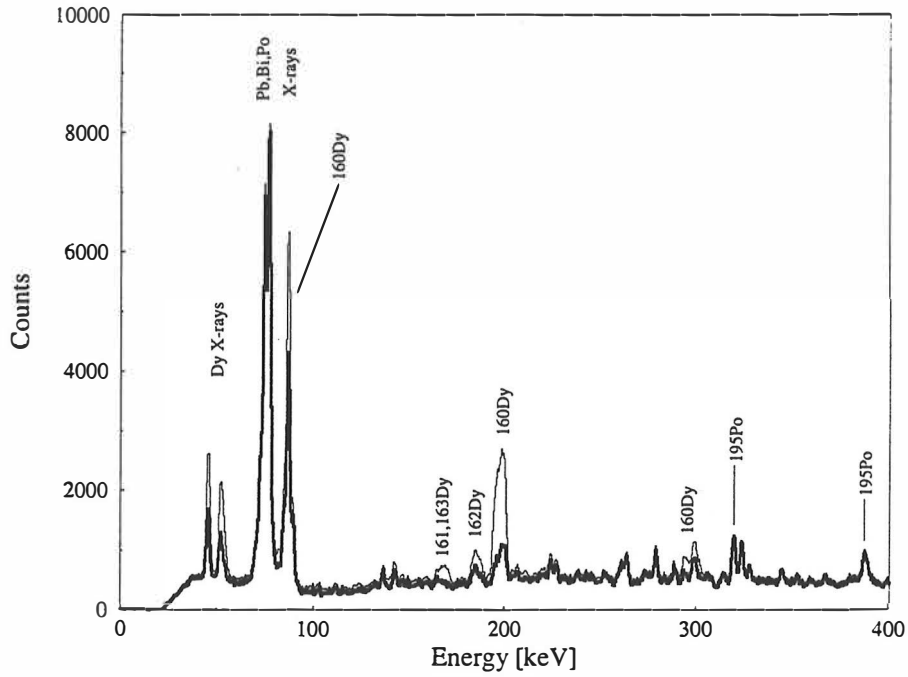

Figure 3.8. A part of the γ-ray spectrum from the ^{36}Ar (178 MeV) + ^{160}Dy -> ^{196}Po* reaction gated with prompt recoil-γ peak (thin line) and the same spectrum when the background due to random recoil - γ events is subtracted (thick line).

3.3.2 Recoil – decay tagging

The idea of the recoil-decay tagging (RDT) method is to identify a recoil detected at the separator focal plane by using its known, characteristic radioactive decay

properties and to single out the prompt γ rays emitted by this recoil. Recoil-decay tagging is utilized when the amount of nuclei of interest is very small compared to other reaction products and the nucleus decays via charged-particle emission. The successful use of the method requires that the half-life of the decay is short compared to the average time distance between the events in the focal plane detector pixel. The recoil is identified by correlating it in time and space to its subsequent radioactive decay. This identification method was first used at GSI [Sim 86] in connection with the SHIP velocity filter [Sch 79].

All the nuclei studied in this thesis decay via α emission. An α decay is correlated with a recoil implantation if it is detected at the same position in the detector within a certain time interval. This interval is determined by the half-life of the α-decaying recoil. When the recoil has been identified the prompt γ rays belonging to it are found by using the recoil-γ TAC as was explained in chapter 3.3.1.

The practical algorithm used in this work for finding correlations between recoils and their α decays is shown in figure 3.9. The two important parameters used in the correlation analysis are time and position of an event. The time for each event is obtained from its clock stamp.

In the analysis each Si detector event is tested whether its energy passes either the recoil or α gate. If a recoil event is found all the important parameters (time, γ-ray energies in the same event, recoil-γ TAC signal) are stored into a two dimensional table according to its position coordinates. Afterwards, when an α particle with a suitable energy passes the α gate a recoil in the same strip is searched back in time around the position where the α was found. The width of the search area is determined by the recoil-α distance distribution obtained from the calibrations and is usually of the order of 500 μm in both directions from the α position. Of those recoils found within this distance range the one closest in time is chosen. The parameters of the chosen recoil are restored and the γ rays are recoil gated. A result from this procedure in an optimal case is a clean γ-ray spectrum consisting of γ transitions originating from a single type of isotope.

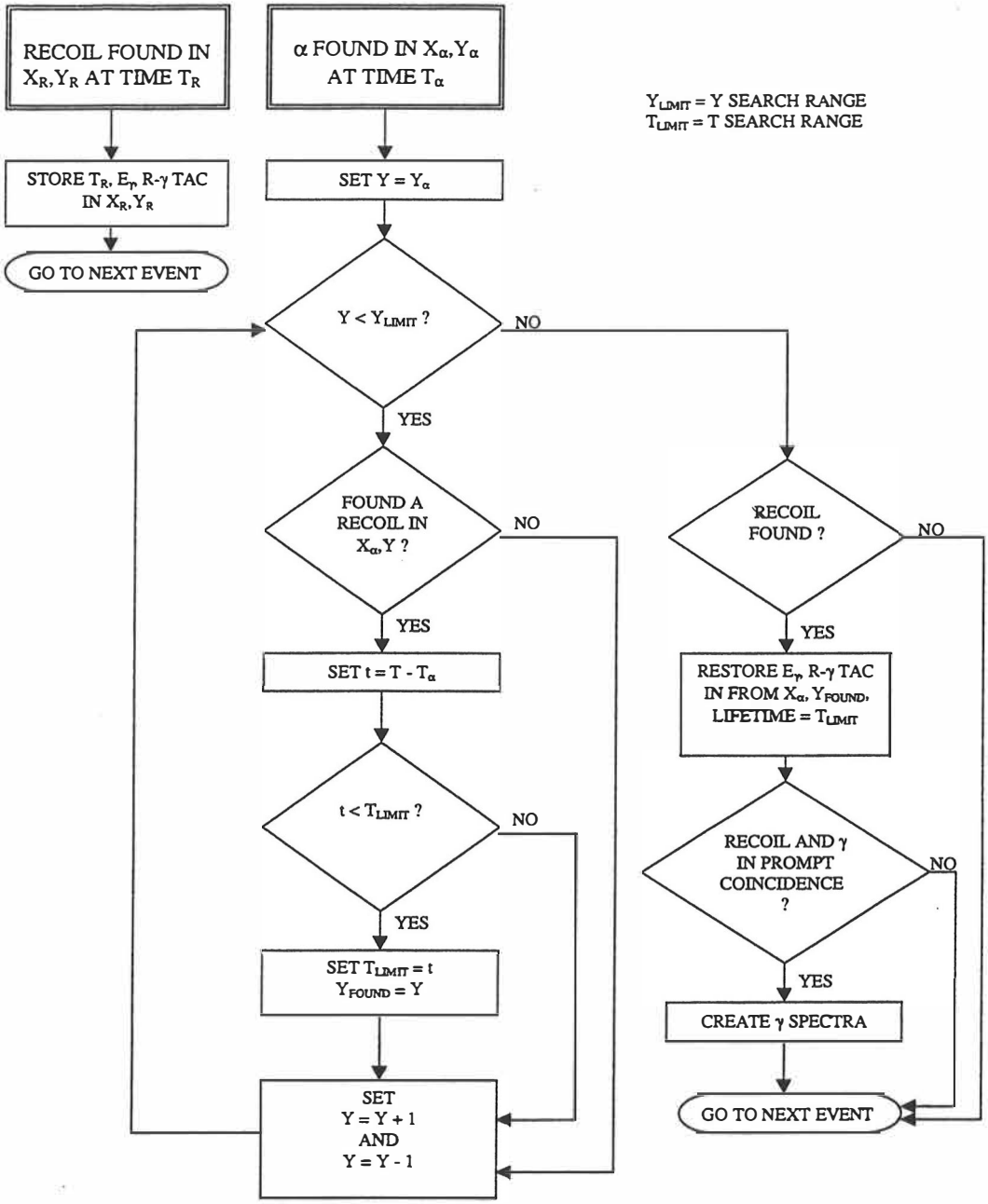

Figure 3.9. The algorithm used for recoil-decay tagging. $X_{\alpha,(R)}$ and $Y_{\alpha,(R)}$ are the horizontal and vertical position of an α particle (recoil) observed in the focal plane detector at time $T_{\alpha,(R)}$.

An example of the power of the RDT method is given in figures 3.10 a), b) and c). The spectra are from the reaction ^{36}Ar (178 MeV) + ^{160}Dy $\rightarrow$ ^{196}Po* and are obtained by using the DORIS + RITU setup. Figure 3.10 a) shows all the γ rays observed by the DORIS array. In 3.10 b) the γ rays are recoil gated and thus the biggest peaks seen in the spectrum originate from the dominating fusion-evaporation channels. In this case the main α-decaying fusion-evaporation residue was ^{195}Po produced by the impurities in the ^{160}Dy target (see fig. 3.3). The spectrum in 3.10 c) shows the γ rays tagged with ^{192}Po α decays. The effective number of pixels in this experiment was about 115. Because the total counting rate of the detector was ~150 s^{-1} the counting rate per pixel was ~1.3 s^{-1} making the average time distance between the events in a pixel ~770 ms. This is much longer than the half-life of ^{192}Po, 33.2±1.4 ms [Bij 96] and therefore the amount of accidental correlations is very low in this analysis, resulting in a clean ^{192}Po γ-ray spectrum. The resolving power can be discussed also by the means of the γ counting rates. The total rate for the γ events stored to the tape was ~900 per second. At the same time the total rate of ^{192}Po γ rays found in the RDT analysis was ~1 per minute and the rate of ^{192}Po 2^{+}-0^{+} transitions was ~3 per hour. In other words, the RDT analysis picked up about 0.002 % of the total γ rays (fig. 3.10 a)) to create the spectrum in figure 3.10 c).

If the counting rate in the Si detector is high such that the time between events in one detector pixel is short compared to the half-life of the recoil nucleus of interest the background in the recoil-decay tagged spectrum increases. This is due to the accidental correlations caused by the random events passing the energy and time gates. The nature of the background γ-ray peaks appearing in the spectrum depends on the major source of the recoil background. For scattered beam or target like particles the γ-rays originate from target Coulomb excitation or other major γ-ray sources at the target position. If the counting rate in the focal plane detector is dominated by some fusion reaction product different from the recoil of interest the γ-ray background originates from this major fusion-evaporation product.

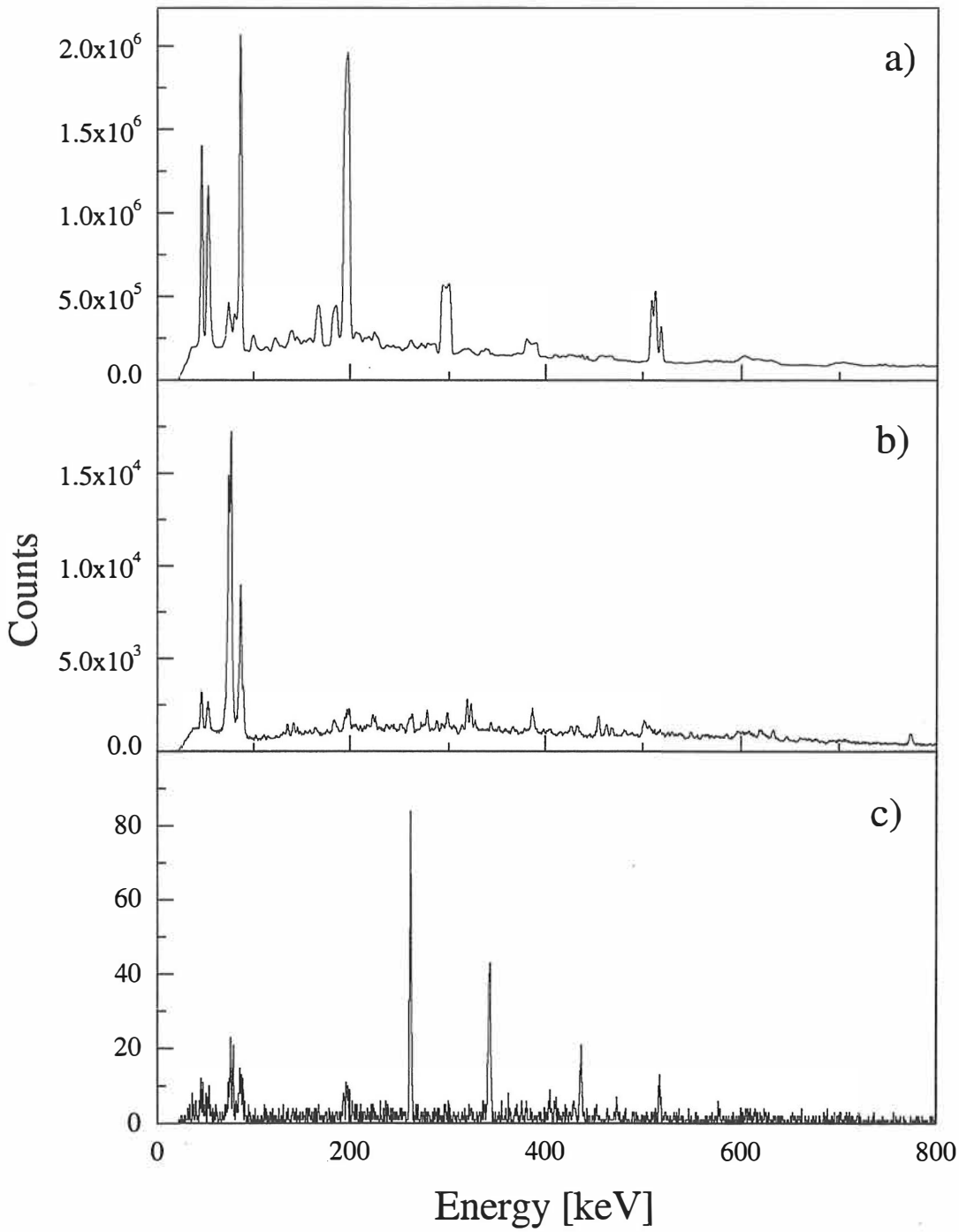

Figure 3.10. a) Singles γ ray spectrum detected by DORIS array from the ^{36}Ar (178 MeV) + ^{160}Dy reaction b) γ-ray spectrum gated by separated recoils c) γ-ray spectrum extracted by tagging with the α decay of ^{192}Po.

The amount of accidental correlations can be estimated by using the formula [Sch 84]

$$N_{acc} = Dr_R(1 - e^{-r_\alpha T}) \tag{3.1}$$

where D is the duration of the experiment, r_α and r_R are the average counting rates in the detector for α particles and recoils, respectively and T is the searching time used in the correlation analysis. If $r_\alpha T << 1$ the formula simplifies to

$$N_{acc} = Dr_R r_\alpha T = n_R n_\alpha T / D \tag{3.2}$$

where n_α and n_R are the total number of α particles and recoils, respectively.

The nucleus ^{176}Hg was studied with the Jurosphere + RITU setup using the ^{36}Ar (190 MeV) + ^{144}Sm → ^{176}Hg + 4n reaction [Mui 98]. The main reaction product was ^{176}Pt,

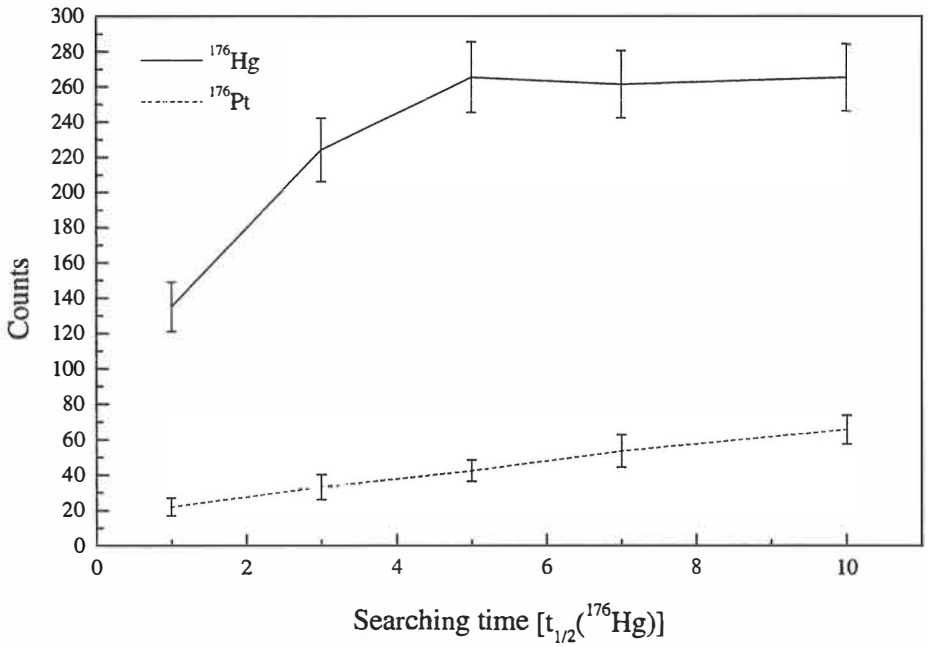

Figure 3.11. Observed γ-ray intensities of the $2^+ \rightarrow 0^+$ transitions in ^{176}Hg and ^{176}Pt as a function of searching time in ^{176}Hg α tagged γ-ray spectrum.

which was produced about 700 times more than ^{176}Hg. Even though the half-life of ^{176}Hg is short, 21±3 ms the high counting rate of ^{176}Pt recoils causes accidental correlations and thus leaking of ^{176}Pt γ-ray peaks into the recoil-decay tagged ^{176}Hg spectrum. In figure 3.11 the intensities of the 2^+ - 0^+ transition peaks of ^{176}Hg and ^{176}Pt from the ^{176}Hg α tagged γ-ray spectrum are plotted as a function of the searching time. The amount of the ^{176}Pt γ-ray events is growing linearly with the searching time as is expected according to equation 3.2. At the same time the intensity of the ^{176}Hg γ peak grows as $1 - 2^{-n}$, where n is the number of half-lives used as a maximum searching time.

3.3.3 Methods for γ-ray detection at the focal plane of RITU

If an additional Ge detector (or several of them) is placed close to the focal plane Si strip detector γ rays from long-living isomeric states in the separated recoil nuclei, as well as γ rays emitted from α and β decay products can be detected. An additional TAC is set up to measure the time between the events in the Si strip detector and the focal plane γ-ray events. The focal plane Ge detector(s) can be used independently of the recoil detection if the nucleus of interest is the main γ-ray emitter at the focal plane. In many cases, however, additional methods for identifying these γ rays are needed.

Recoil-decay tagging at the focal plane

A recoil-decay tagging procedure discussed in chapter 3.3.2 can be utilised also to tag the isomeric γ-ray transitions. In this case the focal plane γ rays occurring in the same event with the identified recoil are used to create a spectrum. The half-life of an isomeric state is obtained using the recoil-decay tagged time distribution between the Si detector and focal plane γ events measured by the TAC unit.

Recoil-decay tagging for very delayed γ rays

If the half-life of the isomeric state is very long (longer than an event in the data acquisition, determined by the width of the master trigger) most of the associated

delayed γ rays detected by the focal plane Ge detector do not end up in the same event with the recoil. In this case, in addition to the recoil-α correlation one has correlated delayed γ rays with the associated recoils. As the γ-ray detection does not involve any position information this is done in practice by selecting the first γ ray event after the implantation of an α correlated recoil. This method is feasible only if the γ counting rate due to the interesting γ rays is much higher than the background γ counting rate.

Isomer γ tagged prompt γ rays

In the case where the γ decay of an isomeric state is well known and information on the excited states above the isomer is missing one can use delayed γ rays to tag the prompt γ rays. The timing information is obtained by using the prompt and delayed recoil-γ TACs. In this method a matrix of prompt and delayed γ rays occurring in the same event is formed. The prompt transitions are identified by setting gates on the delayed γ ray axis of the matrix. This method [Cul 98], as well as the previously discussed method of RDT for very delayed γ rays was not used in this work.

4. POLONIUM NUCLEI

4.1 Introduction

Even though the Pb nuclei have a closed proton shell of Z = 82 and should thus exhibit spherical shapes, coexisting deformed states at low excitation energies have been observed in light Pb isotopes [Woo 92]. Similar shape coexistence phenomena are also seen in Hg and Pt nuclei having Z < 82. In all these elements the deformed states minimize their energy near the neutron midshell at N = 104. In Pb, Hg and Pt nuclei the origin of these deformed intruder states is supposed to be the interaction of the open neutron shell with proton particle-hole excitations across the Z = 82 shell gap.

Due to experimental difficulties, information on the very neutron-deficient nuclei with Z > 82 is still scarce and thus the existence of shape coexistence in these nuclei has not been verified. In this respect the Po nuclei [Cur 98] with two protons outside the Z = 82 shell form an interesting series of isotopes. In Nilsson-Strutinsky calculations May et al. [May 77] have predicted a coexisting oblate deformed minimum to come down in energy in light Po isotopes and reach the ground state in ^{192}Po.

The excited levels in the neutron-deficient Po nuclei down to N = 108 have previously been studied using both in- and off-beam γ-ray detection and α-decay methods [Fir 96], [Maj 90], [Alb 91], [Bij 95], [You 95], [Hel 96], [Bij 98]. An abrupt drop of the level energies is observed in Po isotopes with N ≤ 114. Alber et al. [Alb 91] associated it with deformed proton *4p-2h* configurations intruding down in excitation energy. The α- and β-decay studies by the Leuven group [Bij 95], [Bij 98], [Wau 92], [Wau 94], [Bij 96] strongly support this view and the picture that the observed level structure results from mixing of the normal and intruder states at low spins.

However, the Rutgers group has presented an alternative explanation, based on observed quadrupole vibrational features of ^{198}Po and ^{196}Po [Ber 95]. Their view is that instead of the *4p-2h* proton configurations, the neutron orbitals, especially $i_{13/2}$,

are responsible for the sudden energy changes. The further depression of the level energies in ^{192}Po and ^{194}Po is taken as a sign of an evolution towards a more collective, anharmonic vibrator [You 95], [Fot 97a]. Younes et al. [You 97] have also succeeded to reproduce the low-energy level structure of the neutron-deficient Po nuclei quite well in the particle-core model (PCM) calculations based on the assumption of two protons outside the Z = 82 shell closure coupled to a vibrating core. However, the behavior of the excited 0^+ states could not be explained with this model.

Recently, Oros et al. [Oro 99] have used several theoretical approaches to model the behavior of neutron-deficient Po nuclei. Their calculations support the view of mixing of two coexisting structures to be responsible for the observed perturbation of the energy levels in light Po nuclei. On the other hand, they conclude that the PCM model can predict quite well the experimentally observed level properties of Po isotopes with A = 200 - 210. However, it is not able to reproduce the changes happening in the N < 116 Po isotopes with physically meaningful parameters.

In our earlier work excited states up to $I^{\pi} = 8^+$ in ^{192}Po [Hel 96] were observed for the first time revealing signs of flattening of the level-energy systematics when going towards the neutron midshell. A similar behavior of level energies has been observed in even-mass Pt nuclei where it has been interpreted as an evidence for a ground state intruder configuration [Woo 92]. Based on this observation and the mixing calculations performed by Bijnens et al. [Bij 96] the observed excited states of ^{192}Po were assigned to a deformed intruder ground-state band. The measurement for the excited states of ^{192}Po was repeated by Fotiades et al. [Fot 97a].

Study of odd-mass Po nuclei provides an alternative tool for the examination of shapes of Po isotopes. Fotiades et al. [Fot 97b] have studied the light odd-mass $^{193-197}$Po nuclei and come to the conclusion that in these nuclei the odd $i_{13/2}$ neutron is weakly coupled to a vibrating core. This neutron increases collectivity which is mainly anharmonic vibrational in character.

In order to shed light on the ambiguities discussed above we have performed a γ-ray spectroscopic study of light odd- and even-mass Po nuclei with N = 108 - 111. Due to strong fission competition, the fusion-evaporation reaction channels for populating these Po nuclei become very weak. Therefore, special triggering methods are needed to resolve the events of interest from the vast background. In the present work the $^{192-195}$Po nuclei are studied utilizing the recoil-decay tagging (RDT) [Sim 86], [Pau 95] and recoil gating methods for both prompt and delayed γ rays. The level schemes are extended from the previous ones [You 95], [Hel 96], [Fot 97b] giving a possibility for new evaluations on the structure of light Po nuclei.

4.2 Experiments

The polonium nuclei studied in this work were produced in several experimental runs. The in-beam γ-ray data were acquired in four experiments. These experiments resulted in new information on excited states of $^{192-195}$Po [Hel 99]. Excited states in ^{192}Po were identified for the first time. Results of the preliminary analysis were published earlier in a short report [Hel 96]. Some of the data on the isomeric states have been obtained as a side product from the experiments focussed on the α-decay studies of the neutron-deficient odd-mass polonium nuclei ^{191}Po and ^{193}Po [And 99a], [And 99b]. In these runs the γ-ray detection system was behind the focal plane particle detector and no prompt γ-ray data were recorded. Details of all the experiments are collected in table 4.1.

The experiments were carried out in the accelerator laboratory of the University of Jyväskylä (JYFL) and the beams were provided by the JYFL cyclotron. In all the runs the gas-filled recoil separator RITU [Lei 95] was utilized in connection with a γ-ray detection system installed around the target area and/or at the focal plane. The target thicknesses were about 500 μg/cm^2 in all of the runs to enable the fusion-evaporation residues to fly from the target to the separator and to optimize the yield with respect to their angular spread. In the prompt γ-ray detection, two different Compton suppressed Ge detector systems, DORIS and Jurosphere were used. Thin

copper (0.5 mm or 1 mm) or tin (0.25 mm) plates were set in front of the Ge detectors to reduce the counting rate due to target X-rays. The maximum counting rates in the Ge detectors around the target position were about 10 kHz. Two focal plane Ge detector setups were utilized: either a single 25% Ge, positioned at 2 cm distance from the silicon detector, or an array of four 25% Ge detectors at about 6 cm from the Si detector. For enabling a close geometry the Ge detectors on the focal plane were not Compton suppressed.

Table 4.1. Details of the experiments.

Exp.#	Beam	E_{beam} (MeV)	I_{beam} (pnA) [a]	Target (enrichment)	Nuclei studied [b]	γ detection mode	γ detector setup	Si detector strips	Si counting rate [a]
1	^{36}Ar	178	20	^{160}Dy (70%)	**^{192}Po**, ^{193,195}Po	In-beam	DORIS	8	150 Hz
2	^{28}Si	143	25	^{170}Yb (72%)	**^{194}Po**, ^{195}Po	In-beam	DORIS	8	300 Hz
3	^{28}Si	155	25	^{171}Yb (90.4%)	**^{194}Po**, ^{195}Po	In-beam	DORIS	8	200 Hz
4	^{28}Si	155	20	^{171}Yb (90.4%)	**^{194}Po**, ^{195}Po	In-beam, delayed	Jurosphere, 25% Ge	16	130 Hz
5	^{36}Ar	196 [c]	[c]	^{160}Dy (70%)	(**^{191}Po**,) ^{192}Po	Delayed	25% Ge	16	[d]
6	^{32}S	172	30	^{166}Er (>96%)	(**^{193}Po**,) ^{194}Po	Delayed	4*TESSA	16	230 Hz

[a] Beam intensities (given in units of particles nA) and counting rates are approximate average values.

[b] The nucleus of main interest in the run is marked with bold letters. Nuclei shown in parentheses are not discussed in this work.

[c] The beam energy and intensity had several values during the experiment. The maximum energy was 196 MeV.

[d] The counting rate varied much as a function of beam energy and intensity.

4.3 Experimental results

4.3.1 ^{192}Po

Prompt γ rays from ^{192}Po were collected in experiment 1 (see table 4.1). The results from the preliminary analysis of the data are published earlier in the short report [Hel 96]. During this experiment, a total of about 35000 ^{192}Po α decays were detected in 120 hours. A half-life of 32.2(3) ms for the ^{192}Po α decay was extracted, being consistent with the value 33.2(14) ms given in literature [Bij 96]. An RDT analysis was performed resulting in the prompt ^{192}Po γ-ray spectrum shown in figure 4.1. The energies and intensities of the observed γ-ray transitions are listed in table 4.2.

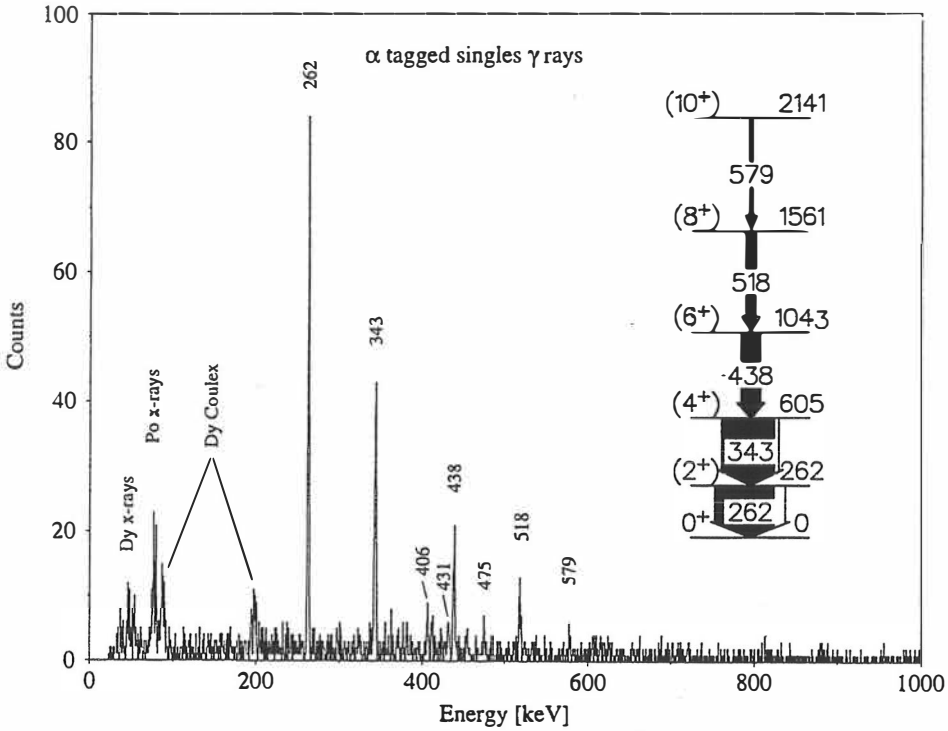

Figure 4.1. Singles γ-ray spectrum tagged with ^{192}Po α decay. The deduced level scheme of ^{192}Po is as an inset.

Table 4.2. γ-ray transitions and energy levels in ^{192}Po.

E_γ (keV)	Intensity (%)	E_i (keV)	J_i (ħ)	J_f (ħ)
262.0(3)	100(6)	262	(2^+)	0^+
343.2(3)	89(8)	605	(4^+)	(2^+)
438.1(5)	32(5)	1043	(6^+)	(4^+)
517.9(5)	17(5)	1561	(8^+)	(6^+)
579.4(5)	6(2)	2141	(10^+)	(8^+)
406(1)	9(3)			
431(1)	8(2)			
475(1)	6(2)			

Also an α tagged matrix of γγ coincidences was created. Even though the number of events in this matrix was small, coincidences between the three lowest transitions could be seen revealing their cascade character. The level scheme shown as an inset in figure 4.1 was constructed supposing that the 262, 343, 438, 518 and 579 keV transitions form an E2 cascade. Ordering of the transitions was based on their observed intensities. Due to the lack of statistics the spin assignments are based on the energy level systematics. According to our assignments levels up to 10^+ are seen. A set of weaker γ rays at energies 406, 431 and 475 keV can also be assigned to ^{192}Po but cannot be placed into the level scheme.

Experiment 5 focussed on the study of the α decay of ^{191}Po. However, about 8500 α particles belonging to the ^{192}Po decay were observed. An RDT method for the focal-plane Ge detector was utilized to search for possible delayed γ-rays from ^{192}Po. The $2^+ \rightarrow 0^+$, $4^+ \rightarrow 2^+$ and $8^+ \rightarrow 6^+$ γ-ray transitions of ^{192}Po were clearly seen in the resulting spectrum. The $6^+ \rightarrow 4^+$ transition was missing, probably due to the insufficient statistics. The observation of these transitions is an indication of the existence of an isomeric state above the 8^+ state having a half-life of the order of one microsecond. No quantitative analysis on the energy or the half-life of the isomer was possible.

4.2.2 ^{193}Po

In-beam γ-ray data for ^{193}Po were collected as a side product in experiment 1. The nucleus ^{193}Po has two α-decay branches, one from the $3/2^-$ state (E_α = 6.949 MeV, $t_{1/2}$ = 0.45 s) and the other from the $13/2^+$ state (E_α = 7.004 MeV, $t_{1/2}$ = 0.24 s) [Wau

93]. The energies of these states relative to each other are not known. About $9 \cdot 10^4$ α particles from ^{193}Po were detected in total, $3 \cdot 10^4$ of them from the decay of the $3/2^-$ state. An RDT analysis was performed for both of the α-decay branches resulting in the prompt γ-ray spectra shown in figure 4.2 a) and b). The energy resolution of the Si detector was not good enough to fully separate the two α peaks. Moreover, the relatively long half-lives resulted in increased amount of accidental correlations in the correlation analysis, thus increasing the number of background events in the γ-ray spectra. The energies and intensities of the γ-ray transitions assigned to ^{193}Po are listed in table 4.3. The intensities are normalized to the most intense γ-ray transition in each spectrum.

A matrix of coincident γ-ray transitions tagged by the α decay from the $13/2^+$ state was constructed. The spectra with gates on the three strongest lines (251, 361 and 464 keV) clearly show that these transitions are in coincidence with each other. The sum of the gated spectra is presented in figure 4.3. The level scheme built on top of the $13/2^+$ state of ^{193}Po is shown as an inset in Fig. 4.2 b). The yrast band in the level scheme was built by using the intensity and coincidence information of the γ rays. The tentative spin assignments are based on the energy level systematics. The nonyrast part of the level scheme is based on the energy sums and intensities of the γ rays and is thus marked tentative.

A few γ-ray transitions were seen also on the top of the $3/2^-$ state of ^{193}Po (fig. 4.2 a)). Due to low statistics and the lack of coincidences, construction of a level scheme was not possible.

The excited states in ^{193}Po have previously been studied by Fotiades et al. [Fot 97b]. The observation of γ-ray transitions above the $13/2^+$ state with energies of 251, 361, 368 and 486 keV was reported but the proposed level scheme differs from the one of this work. A transition of 234 keV, tentatively placed above the $3/2^-$ state, was not seen in our data.

Table 4.3. γ-ray transitions and energy levels in ^{193}Po.

E_γ (keV)	Intensity (%) [a]	E_i (keV)	J_i (ħ)	J_f (ħ)
γ-ray transitions above the $3/2^-$ state:				
206.7(5)	100(20)			
349.1(5)	100(40)			
367(1)	50(20)			
γ-ray transitions and energy levels above the $13/2^+$ state:				
251.4(5)	100(7)	251	$(17/2^+)$	$13/2^+$
274.9(5)	21(4)	(275)	$(15/2^+)$	$(13/2^+)$
360.9(5)	59(7)	611	$(21/2^+)$	$(17/2^+)$
369(1)	18(5)	(644)	$(19/2^+)$	$(15/2^+)$
393(1)	15(4)	(644)	$(19/2^+)$	$(17/2^+)$
463.7(5)	22(6)	1075	$(25/2^+)$	$(21/2^+)$
485(1)	15(5)	(1129)	$(23/2^+)$	$(19/2^+)$
518(1)		(1129)	$(23/2^+)$	$(21/2^+)$
549(1)	12(4)			
574(1)	7(3)			

[a] The intensities are normalised to the strongest transition in both spectra.

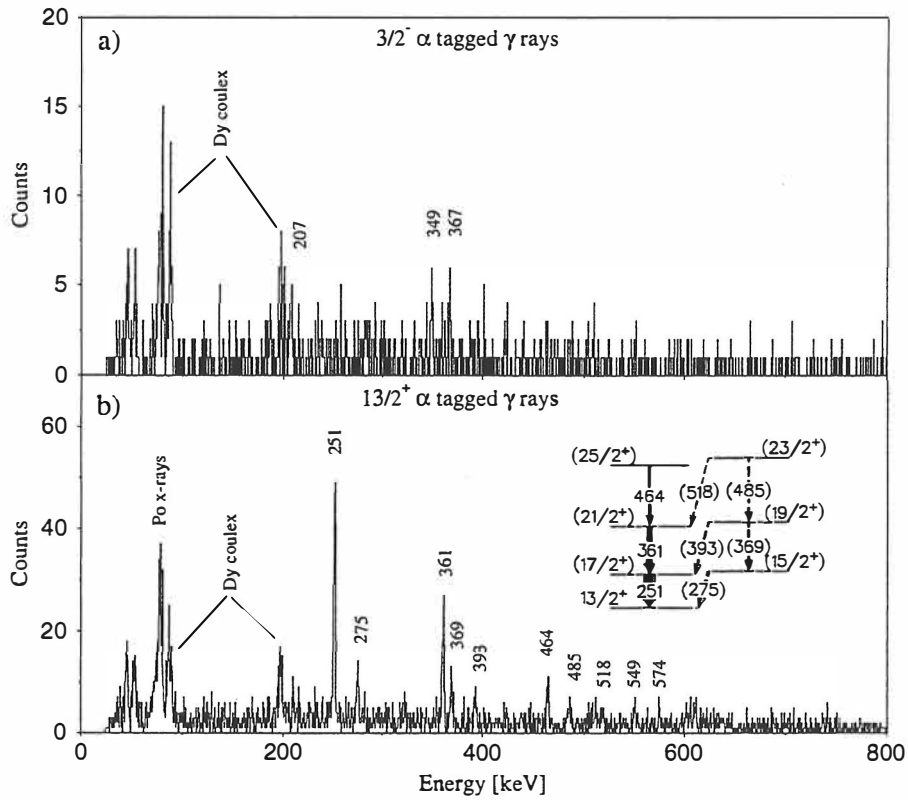

Figure 4.2. a) A singles γ-ray energy spectrum tagged with the α decay from the $3/2^-$ state of ^{193}Po. b) A singles γ-ray energy spectrum tagged with the α decay from the $13/2^+$ state of ^{193}Po. The deduced level scheme above the $13/2^+$ state is as an inset.

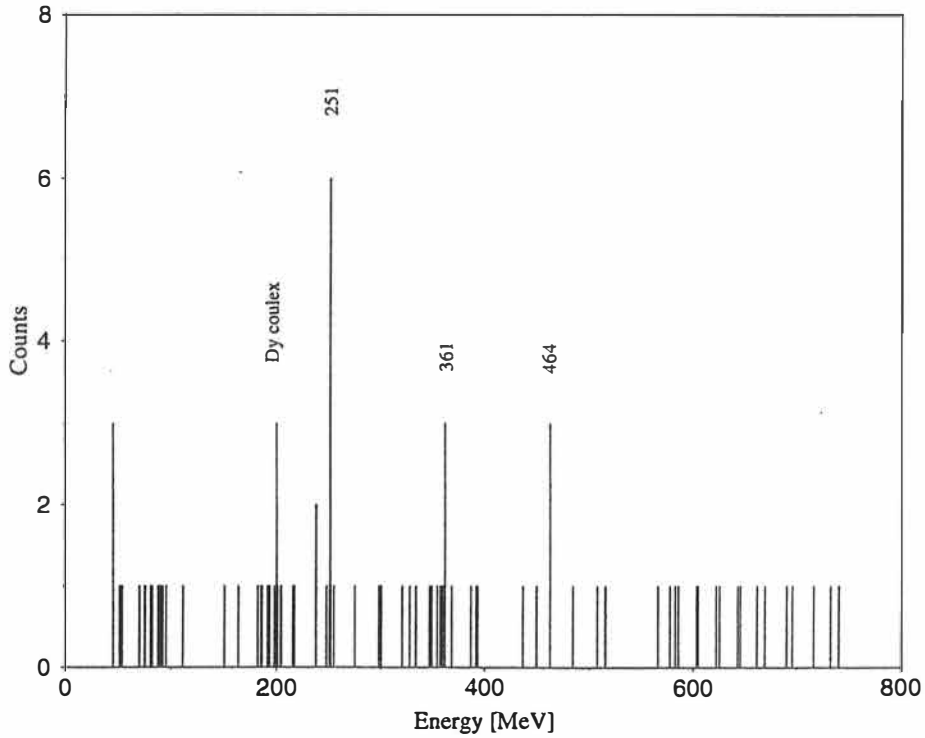

Figure 4.3. Sum of the spectra gated by the 251keV, 361keV and 464keV transitions of ^{193}Po.

4.2.3 ^{194}Po

The in-beam γ-ray data on ^{194}Po were collected in three runs dedicated to the production of this nucleus (experiments 2 - 4). In these runs a total of about 2 million ^{194}Po α decays was detected in about 12 days. The α spectrum from experiment 4 is shown in figure 4.4. The data from all of the experiments were put together and analysed using both the RDT and recoil-gating methods. The ^{194}Po half-life resulting from the analysis, 370(40) ms, is consistent with the literature value of 392(4) ms [Wau 93]. The total α tagged singles γ-ray spectrum for ^{194}Po is shown in figure 4.5 a). Two γγ coincidence matrices were constructed, one from α tagged γ rays of ^{194}Po and the other from all the recoil gated γ rays. The level scheme of ^{194}Po was built by analysing these matrices with the RADWARE software package [Rad 95]. The α tagged γ rays of ^{194}Po from experiments 2 and 3 were sorted into two singles spectra, the other one consisting of the γ rays observed in the detectors at angle 143°

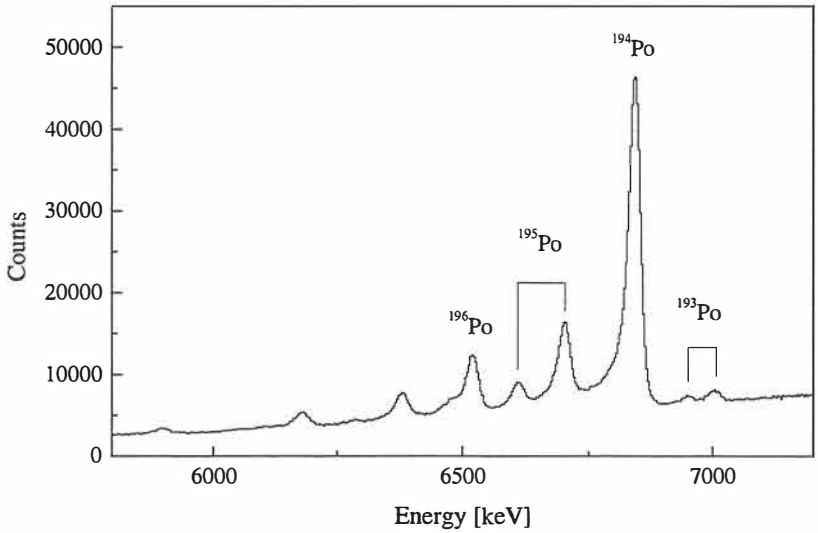

Figure 4.4. The α spectrum from reaction $^{28}Si + ^{171}Yb \rightarrow ^{199}Po^*$.

and the other one of those observed in the detectors at angles 78° and 102°. The spin assignments were based on the angular distributions of the γ-ray transitions measured as the ratio I(143°)/I(~90°) and on the level systematics. The I(143°)/I(~90°) ratio for the well-known stretched E2 transitions in ^{196}Po seen in the same experiment was 1.20(8). The level scheme consists of an yrast band extending to $I^{\pi} = (16^+)$ and a side band of low-lying 2^+_2, 4^+_2 and 6^+_2 states and odd-spin negative-parity states 7^- and 9^-. The sum of the spectra gated by the 545 keV and 602 keV peaks (fig. 4.5 b)) reveals the yrast transitions. The sum of the 434 keV and 454 keV gates is presented in figure 4.5 c), showing other prompt transitions placed in the level scheme (except the 959 keV transition not seen in either of these gates). A 319 keV γ–ray transition was seen in coincidence with the 320 keV $2^+_1 \rightarrow 0^+_1$ transition but could not be placed into the level scheme, as well as the prompt γ-ray transitions of 359 keV and 803 keV.

The data on the isomeric state of ^{194}Po were obtained as a side product of the ^{193}Po α-decay experiment (experiment 6), where a total of about $1.7 \cdot 10^5$ ^{194}Po α decays were observed. The RDT method for the delayed γ rays was utilized, resulting in the

spectrum shown in fig. 4.5 d). New γ rays having energies of 373, 459 and 918 keV, not observed in the prompt γ-ray spectrum, were tentatively assigned to form the de-excitation route from an isomeric state, suggested to have $I^{\pi} = 11^{-}$ similar to the isomer in ^{196}Po. A half-life of 15(2) μs was extracted for this state from the recoil-γ time distribution.

Table 4.4. Properties of γ-ray transitions and energy levels in ^{194}Po.

E_γ (keV)	I_γ (%)	E_i (keV)	J_i (ħ)	J_f (ħ)	I(143°)/I(~90°)
292.1(3)	5.1(7)	2917	(14^+)	12^+	
297.7(3)	5.6(9)	2285	9^-	7^-	1.5(4)
319.7(3)	100(8)	320	2^+	0^+	1.22(5)
329.2(3)	7.3(10)	2625	12^+	10^+	1.3(3)
340.8(3)	7.5(12)	1987	7^-	6^+	0.92(13)
359.2(5)	6(2)				0.7(2)
366.5(3)	66(7)	686	4^+	2^+	1.24(7)
371.9(5)	2.8(6)	(2657)	(10)	9^-	0.9(3)
373.1(5)		2066	(8^+)	8^+	
409.9(5)	1.4(5)	(3327)	(16^+)	(14^+)	
433.9(5)	4.9(12)	1646	6^+	4^+	1.2(6)
438.1(5)	6(2)	758	2^+	2^+	1.0(2)
453.9(5)	3.9(11)	1212	4^+	2^+	1.09(10)
458.6(5)		(2525)	11^-	(8^+)	
461.8(3)	43(5)	1148	6^+	4^+	1.30(10)
524.4(5)	5.1(12)	1212	4^+	4^+	0.8(3)
545.2(3)	29(3)	1693	8^+	6^+	1.18(11)
601.8(3)	17(2)	2296	10^+	8^+	1.3(3)
758.1(5)	7(5)	758	2^+	0^+	1.1(3)
802.7(5)	2(1)				0.9(4)
918.3(5)		2066	(8^+)	6^+	
958.7(5)	1.8(0.7)	1646	6^+	4^+	

The level scheme of ^{194}Po based on the present experiments and containing both the prompt and the delayed γ-ray transitions is presented in figure 4.6. The γ-ray energies, intensities, angular distribution ratios, level energies and the spin assignments are collected in table 4.4. Excited states in ^{194}Po were first observed by Younes et al. [You 95]. Their level scheme extended up to a 2625 keV level assigned as an 11^- state and had tentative non-yrast 2^+_2 and 4^+_2 states at the energies 661 keV and 1211 keV. Our results extend the level scheme and information on the intensities of the transitions. According to our new data the 341 keV transition is moved to feed the 1646 keV 6^+ state and the non-yrast 2^+_2 state has an energy of 758 keV. The spin and parity of the 2625 keV state is changed to 12^+, while the 11^- state is isomeric, having a tentative level energy of 2525 keV.

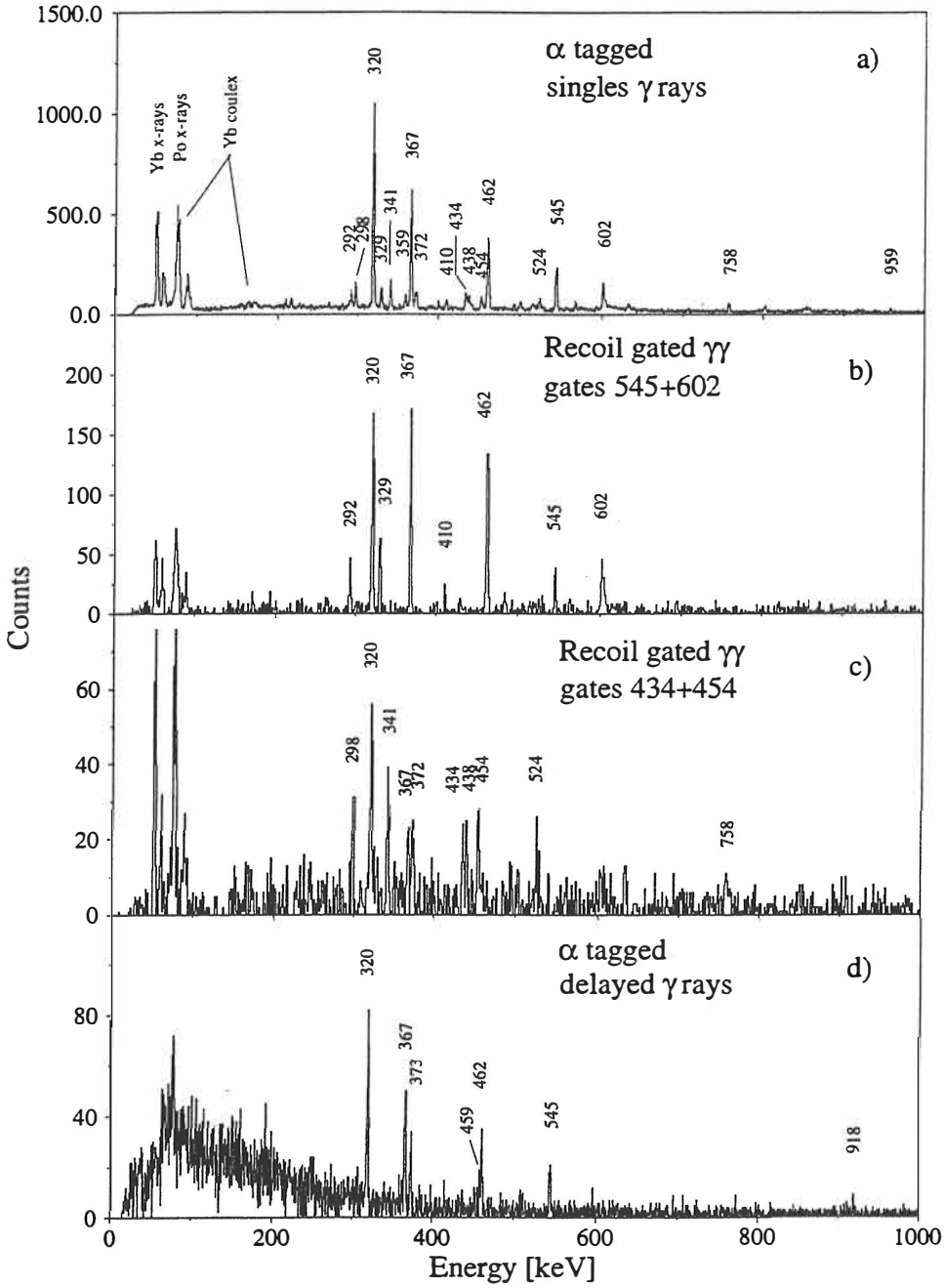

Figure 4.5. a) Singles γ-ray spectrum tagged with the ^{194}Po α decay. b) Sum of the 545.2 keV and 601.8 keV gates set on the recoil gated γγ matrix. c) Sum of the 433.9 keV and 453.9 keV gates set on the recoil gated γγ matrix. d) Spectrum of delayed γ rays observed on the focal plane of RITU and tagged with the ^{194}Po α decay.

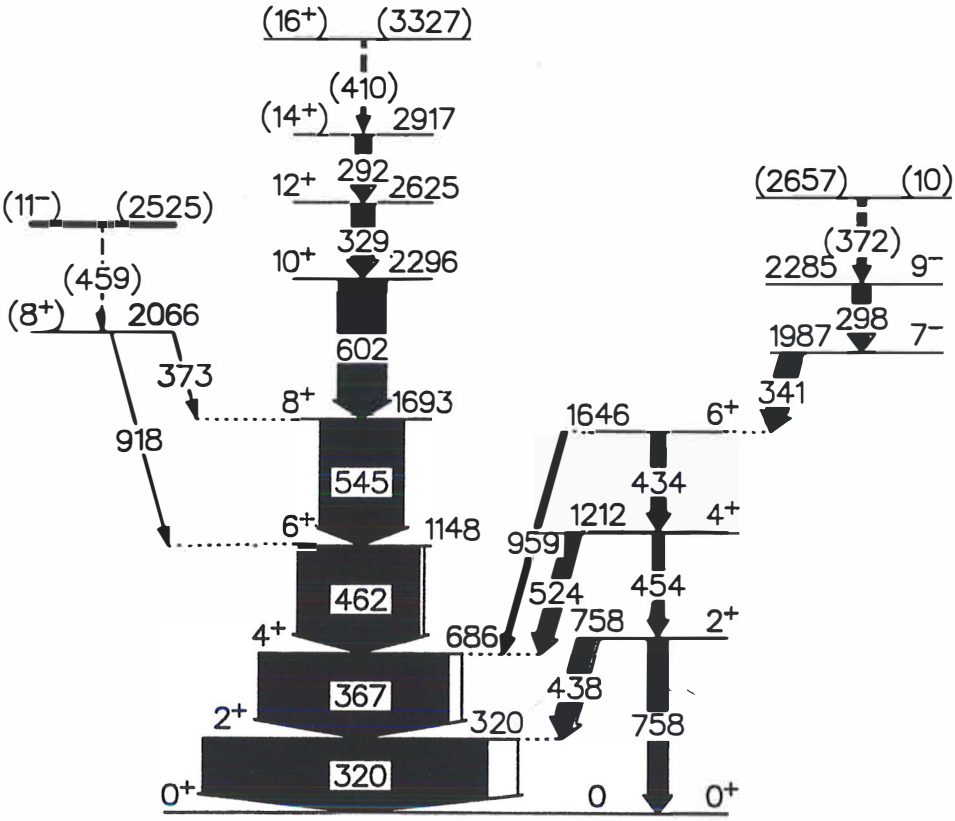

Figure 4.6. Level scheme of ^{194}Po.

4.2.4 ^{195}Po

The data on the excited states of ^{195}Po were collected in in-beam experiments 1 - 4. The nucleus ^{195}Po has two known α decaying states: the $3/2^-$ ground state (E_α = 6606(5) keV, $t_{1/2}$ = 4.64(9) s) and the isomeric $13/2^+$ state (E_α = 6699(5) keV, $t_{1/2}$ = 1.92(2) s) [Wau 93]. The isomeric state lies about 230 keV above the ground state [Fir 96]. A total of about $4 \cdot 10^5$ isomeric and $1 \cdot 10^5$ ground state α decays were observed in experiment 1. The number of α decays observed in experiments 2 - 4 was $1.6 \cdot 10^6$ and $0.4 \cdot 10^6$ for the isomeric and the ground state decay, respectively. An RDT analysis for both of the α decay branches was performed for the prompt γ-ray data from experiment 1. The resulting γ-ray spectra are shown in figures 4.7 a) and b).

The extracted transition energies, intensities, angular distribution ratios, level energies and the spin assignments are listed in table 4.5. As in the case of ^{193}Po the half-lives of the α decays were long considering the average counting rate in a detector pixel. This increased the amount of accidental correlations and thus the background in the γ-ray spectrum. Due to the high counting rate from the main reaction products the recoil-decay tagging analysis for ^{195}Po was not feasible for the data from experiments 2 - 4. However, the strongest transitions above the isomeric $13/2^+$ state were visible in the recoil gated $\gamma\gamma$ matrix. Using this matrix it was possible to observe that the transitions of 319, 388 and 494 keV were in coincidence with each other. In addition, a weak transition of 589 keV was observed in coincidence with the 388 and 494 keV transitions. The angular distributions of the three lowest transitions indicated E2 character for them. Using the γ-ray intensities and the previously mentioned facts as arguments a level scheme shown as an inset in figure 4.7 b) was constructed. Tentatively, a side band similar to that in ^{193}Po could be formed from the 427 keV ($15/2^+ \rightarrow 13/2^+$), 404 keV ($19/2^+ \rightarrow 15/2^+$) and 510 keV ($19/2^+ \rightarrow 17/2^+$) transitions using energy sum and intensity arguments. A tentative level scheme on top of the isomeric $13/2^+$ state of ^{195}Po was previously published by Fotiades et al. [Fot 97b]. Our level scheme confirms their scheme and adds the tentative side band above the $13/2^+$ state and one new level on top of the yrast cascade.

Several weak γ rays were observed in the spectrum tagged with the α decay of the $3/2^-$ ground-state of ^{195}Po (fig. 4.7 a)). However, due to the low statistics it was not possible to order the transitions into a level scheme. The relatively long half-life of the state resulted in a high background. Also for this reason, the observed 319 keV and 387 keV peaks can be originated from the random coincidences with the much more abundantly produced $13/2^+$ state in ^{195}Po. Fotiades et al. [Fot 97b] have reported on three γ transitions above the $3/2^-$ state, having energies of 230 keV, 427 keV and 470 keV. Only the 427 keV transition is clearly seen in our data. Also Taylor et al. [Tay 99] have listed γ transitions seen above the $3/2^-$ state of ^{195}Po. Their list seems to contain most of those transitions reported in both [Fot 97b] and this work.

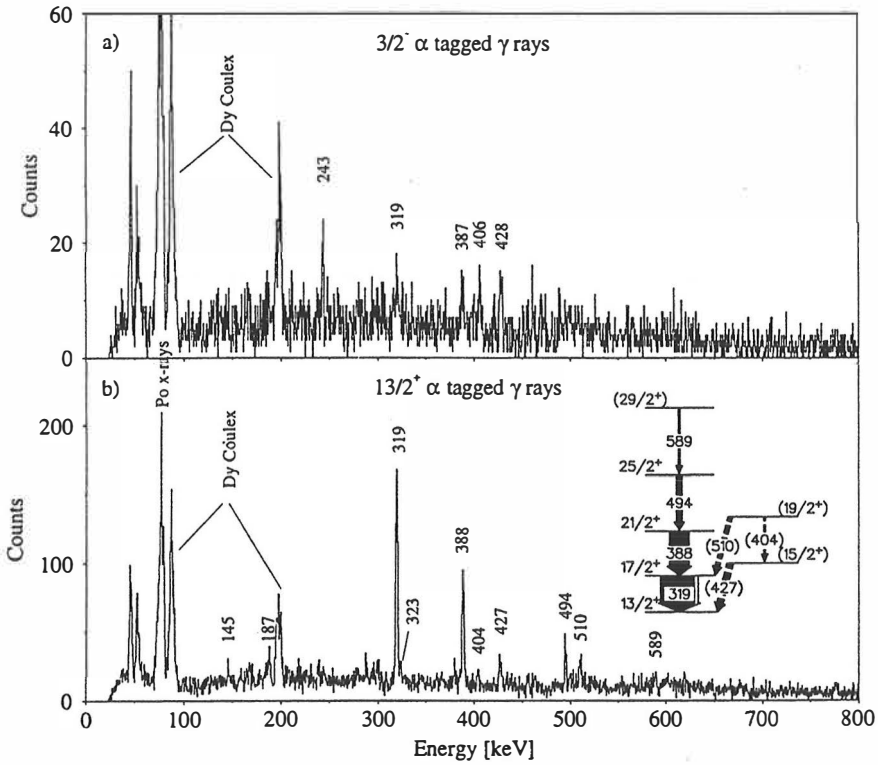

Figure 4.7 a) Singles γ-ray spectrum tagged with the α decay of the 3/2⁻ ground state of ^{195}Po b) Singles γ-ray spectrum tagged with the α decayof the 13/2⁺ isomeric state of ^{195}Po. The deduced level scheme above the 13/2⁺ state is as an inset.

Table 4.5. Properties of γ-ray transitions and energy levels in ^{195}Po.

E_γ (keV)	I_γ (%)[a]	E_i (keV)	J_i (ħ)	J_f (ħ)	I(143°)/I(~90°)
γ-ray transitions above the 3/2⁻ ground state:					
243.2(5)	60(20)				
319(1)	100(13)				
387(1)	61(14)				
406(1)	58(14)				
428(1)	90(30)				
γ-ray transitions and energy levels above the 13/2⁺ isomeric state:					
145(1)	3.7(8)				
187(1)	8.8(1.3)				
319.1(5)	100(4)	319	17/2⁺	13/2⁺	1.5(2)
323(1)	6.1(9)				
388.1(5)	55(4)	707	21/2⁺	17/2⁺	1.5(4)
404(1)	5.7(1.0)	(831)	(19/2⁺)	(15/2⁺)	
426.6(5)	17(2)	(427)	(15/2⁺)	13/2⁺	
494.3(5)	17(3)	1202	25/2⁺	21/2⁺	1.3(5)
510.0(5)	13(3)	(831)	(19/2⁺)	(17/2⁺)	
589(1)	6(2)	1791	(29/2⁺)	25/2⁺	

[a] The intensities are normalised to the 319 keV transition in the both spectra.

4.3 Discussion

4.3.1 Systematics

A level systematics for even-mass $^{192\text{-}210}$Po isotopes including our new data for ^{192,194}Po is shown in figure 4.8. The positive parity low-lying yrast levels of the closed-shell nucleus ^{210}Po are formed by the proton $h_{9/2}{}^2$ multiplet. In the $^{200\text{-}208}$Po isotopes, neutron-hole orbitals are released for 2^+ and 4^+ broken pairs resulting in an increase of collectivity and a decrease of energy of the yrast $2^+{}_1$ and $4^+{}_1$ states. The level-energy behavior is rather smooth until at ^{198}Po, a drop of energies of the $2^+{}_1$, $4^+{}_1$ and $6^+{}_1$ states is observed [Maj 90], [Alb 91], [Ber 95]. The energies of the yrast 8^+ states increase constantly until a sharp drop after ^{196}Po. With these states, in ^{192,194,196}Po also the 10^+ state drops down in energy. A flattening in the level-energy systematics for the yrast levels 2^+ - 10^+ is observed in ^{192}Po. Second excited $2^+{}_2$ and $4^+{}_2$ states have been identified for almost all currently studied Po isotopes.

The smoothly behaving negative-parity states 5^-, 7^- and 9^- were previously assigned as neutron states because of the similarity of their energies compared with similar levels in the Pb isotones [Maj 90]. This similarity seems to weaken in the lighter Po isotopes ^{194,196}Po. Isomeric 11^- states are observed in all the neutron-deficient Po nuclei with $110 \leq N \leq 126$.

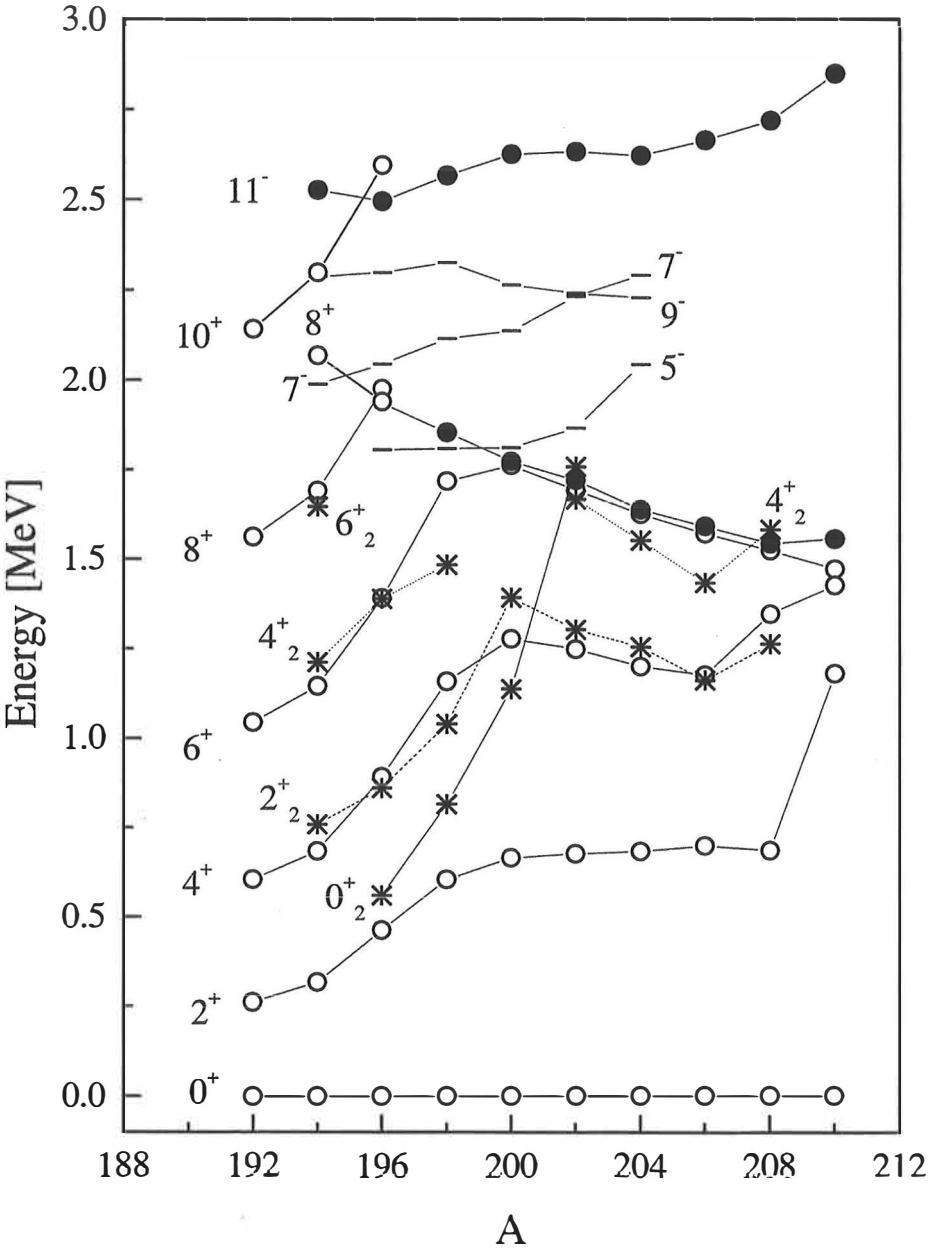

Figure 4.8. Level systematics for even-mass $^{192\text{-}210}$Po isotopes. The yrast positive parity levels are marked with open circles, the non-yrast ones with asterisks and the negative parity levels with bars. The isomeric states are assigned with filled circles.

4.3.2 Vibrational and rotational features

Based on in-beam γ-ray studies, Bernstein et al. have shown that ^{196,198}Po actually have features of quadrupole vibrational nuclei [Ber 95]. The same features are suggested to manifest themselves in ^{194}Po in [You 95]. This interpretation is based on the relatively constant energy spacings of the yrast levels as well as on the appearance of 2^+_2 and 4^+_2 states in the vicinity of the 4^+_1 and 6^+_1 states forming a level structure reminiscent of that of a quadrupole-vibrational nucleus. The model is further argued by the E2 branching ratios determined for the 2^+_2 and 4^+_2 states. If these states were members of two- and three quadrupole-phonon multiplets, respectively, the $2^+_2 \rightarrow 0^+_1$ transition should be forbidden and the B(E2) ratio for the 4^+_2 state should be $B(E2;4^+_2 \rightarrow 2^+_2)/B(E2;\, 4^+_2 \rightarrow 4^+_1) = 1.1$.

For ^{198}Po [Ber 95] and ^{196}Po [Ciz 98] the $B(E2;2^+_2 \rightarrow 2^+_1)/B(E2;2^+_2 \rightarrow 0^+_1)$ ratios are 158(6) and 22(6), and the $B(E2;4^+_2 \rightarrow 2^+_2)/B(E2;4^+_2 \rightarrow 4^+_1)$ ratios 2.0(5) and 1.4(2), respectively, presuming that both branches are of pure E2 character. According to our results the corresponding values for ^{194}Po are 7(3) and 3.7(8). These ratios provide some evidence in support of the phonon picture in ^{194,196,198}Po although the values for ^{194}Po indicate that transition to some other kind of structure sets in.

However, the simple quadrupole vibrator picture for the light Po isotopes is seriously disturbed by the behaviour of the first excited 0^+_2 state, which is observed to intrude down close to the 2^+_1 state in ^{196}Po [Bij 95]. Large anharmonicities would be needed to encounter this state departing from the two-phonon triplet.

A recent study of the de-excitation pattern of the non-yrast 2^+_2 and 0^+_2 states shows that a change in the nature of the low-lying positive parity non-yrast states takes place between the isotopes ^{200}Po and ^{202}Po [Bij 98]. In the heavier isotopes ($A \geq 202$) the positive parity states are assumed to be members of quadrupole phonon multiplets whereas in the lighter isotopes ($A \leq 200$) these states could belong to a deformed band intruding to low energies and mixing with the ground state band.

The yrast band in ^{192}Po and in ^{194}Po with regularly increasing level spacings up to the 10^+ state can be discussed within the framework of a soft rotor. In figure 4.9 the kinematic moments of inertia ($J^{(1)}$) for ^{192}Po and ^{194}Po have been plotted as a function of the γ-ray transition energy. The $J^{(1)}$ values extracted from the transitions above the 2^+ level follow a smoothly increasing trend. This behavior is typical for a soft rotor nucleus and can be described with a variable moment of inertia (VMI). For comparison, the $J^{(1)}$ values for the intruder bands observed in ^{186,188}Pb and in even-A nuclei $^{182\text{-}186}$Hg (Z = 82 - 2) and ^{180,182}Pt (Z = 82 - 4) are shown in the same figure. Similarity between the intruder bands in the even-mass Pt, Hg and Pb isotopes close to the neutron midshell is well known [Dra 94]. These bands have been associated with a prolate minimum predicted in Nilsson-Strutinsky calculations [May 77], [Naz 93]. Figure 4.9 shows how the moments of inertia for ^{192}Po and ^{194}Po behave qualitatively in the same way with the ones in the Pt, Hg and Pb isotopes except that the $J^{(1)}$ values are systematically about 10 $\hbar^2$/MeV lower. The moments of inertia for the yrast band of ^{198}Rn extracted from a recent RDT study [Tay 99], are also shown in figure 4.9 revealing that intruder structures similar to those in ^{192}Po and ^{194}Po also become yrast in very neutron deficient even-mass Rn isotopes. These structures can represent the oblate minimum which according to calculations [May 77] should reach the ground state in ^{192}Po.

The smooth behaviour of the transition energies of the yrast band in ^{194}Po ends when the 10^+ state is passed. Considering this change from the view of the rotational scheme the single-particle alignments (i_x) in a nucleus may be observed when the angular momentum of the collective rotation is subtracted from the total angular momentum. In figure 4.10 this alignment i_x in ^{194}Po is plotted as a function of the rotational frequency $\hbar\omega$. The ground state rotational band with $i_x \approx 0$ persists until at $\omega \approx 0.3$ MeV/$\hbar$ a sharp alignment takes place. The gain obtained in the alignment is about 11 $\hbar$ which is consistent with that for the alignment of two $i_{13/2}$ neutrons.

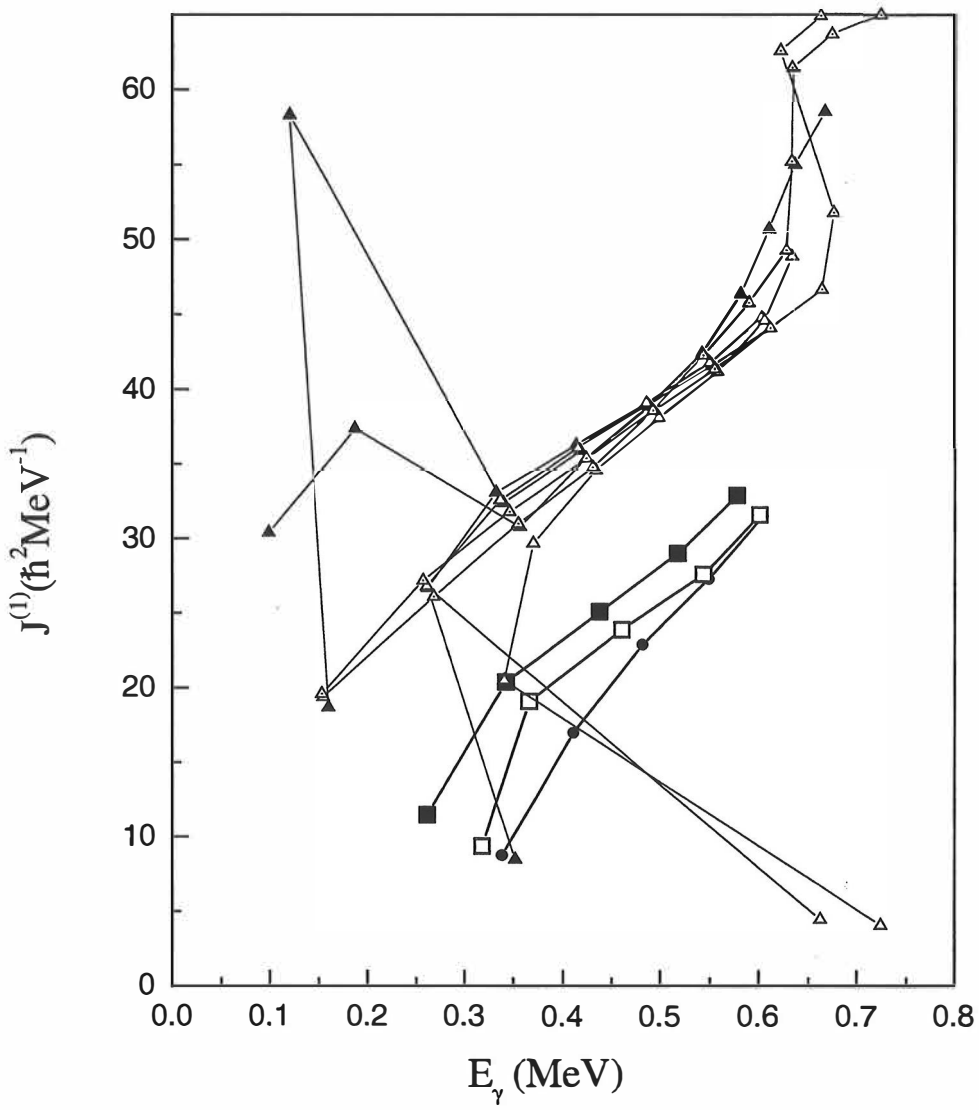

Figure 4.9. Kinematic moment of inertia ($J^{(1)}$) as a function of the γ-ray transition energy for ^{192}Po (solid squares), ^{194}Po (open squares) and ^{198}Rn (circles) compared to several even-mass Pt (triangles with dots), Hg (solid tringles) and Pb (open triangles) nuclei having a prolate deformed band.

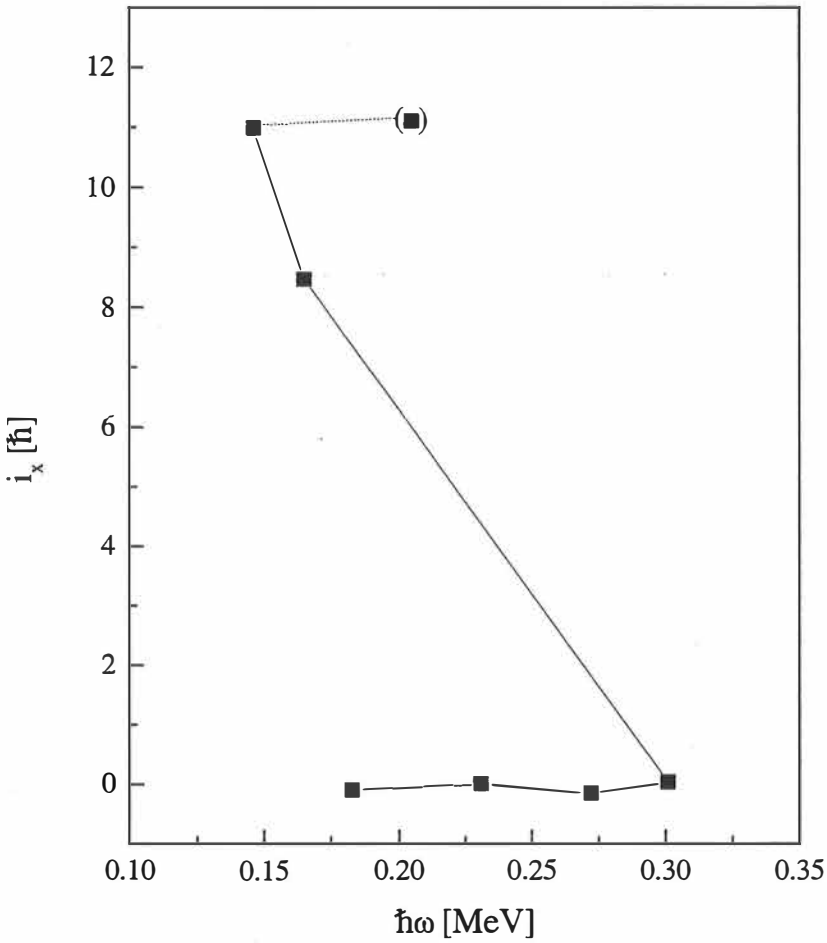

Figure 4.10. Aligned angular momentum i_x for the yrast band in ^{194}Po. A reference with Harris parameters J_0 = 12.8 ħ^2/MeV and J_1 = 205.8 ħ^4/MeV^3 has been subtracted.

4.3.3 Intruder structures

The intruding oblate structures in light Po isotopes are associated with two-proton excitations across the Z=82 gap (*4p-2h* states) [Bij 95]. Based on the simple intruder mechanism an intruder analog scheme was introduced by Heyde et al. [Hey 92]. They suggest that the deformed intruder states can be classified according to their intruder spin which is defined by $I^{(i)} = N_{val}/2$ and $I^{(i)}_z = (N_{val,p} - N_{val,h})/2$, where N_{val} is the number of the valence particle and hole pairs and $N_{val,p}$ ($N_{val,h}$) is the number of the

valence particle (hole) pairs. In this scheme the bosons formed by the particle and hole pairs are treated on the same footing giving rise to intruder spin multiplets with nuclei having similar types of energy level structure. According to this model the rotational bands in Po and Hg isotones, based on the *4p-2h* and *2p-4h* intruder states, respectively, and the ground state band in Os (*6h*), all belonging to the $I^{(i)} = 3/2$ multiplet, should be similar. However, comparison between these bands showed only weak similarities that could also be coincidental. Also the data in figure 4.9, showing the supposed Po intruder bands compared to the observed prolate bands in Hg nuclei disagree with this scheme. The contradiction can be avoided by suggesting that the prolate states in Hg nuclei, similarly to the respective Pb nuclei, belong into even higher excited groups formed by and $I^{(i)} = 5/2$ (*4p-6h* state) multiplets ($I^{(i)} = 2$ or 3 (*4p-4h* or *6p-6h* states) multiplets in Pb) [Naz 93].

This leaves a question about the existence of $I^{(i)} = 3/2$ bands in Hg and $I^{(i)} = 1$ bands in Pb nuclei, especially because the intruder 0^+ states showing *2p-2h* properties are observed in the $A \geq 188$ Pb isotopes in α-decay studies [Dup 84]. On the other hand, while the prolate bands in the intruder spin multiplets of $I^{(i)} = 2$ and $I^{(i)} = 5/2$ are very similar, it can be seen (fig. 4.9) that at high spin the $J^{(1)}$ values of ^{198}Rn, the lightest Z = 86 isotope with known excited states [Tay 99], show the same pattern as the supposed *4p-2h* states ($I^{(i)} = 3/2$) of ^{192}Po and ^{194}Po.

Another analogy scheme for the Pb region is presented by Barrett et al. [Bar 91] who suggest that the shape-coexisting intruder states are members of F-spin multiplets formed by nuclei differing by an α particle. In the F-spin scheme [Ari 77] the valence proton and neutron pairs form bosons having a total F-spin value of $F = (N_\nu + N_\pi)/2$, where N_ν and N_π are the number of neutron and proton bosons, respectively. The multiplet is formed by the nuclei having the same F spin but different projections $F_0 = (N_\nu - N_\pi)/2$. This analogy fits well for the similarity between ^{194}Po and ^{198}Rn (fig. 4.9) but is hard to confirm in ^{190}Pb where no oblate band has been identified.

In the simple picture of the proton intruder states, it rather looks as if the two proton holes in the Z = 82 shell are associated with the oblate minimum (the ground state of even-A Hg, the *2p-2h* 0^+_2 states in Pb with $A \geq 188$, the *4p-2h* state(s) in Po and the

possible *6p-2h* band in ^{198}Rn). In a similar way the prolate shape could be connected to four holes in the Z = 82 shell (prolate bands in Pt, Hg and Pb). The predicted prolate structure in the Po nuclei near the neutron midshell [May 77] could then originate from the *4p-4h* proton excitations across the shell gap. Unfortunately, due to very low production cross-sections it is difficult to probe structures of Z > 82 nuclei close the neutron midshell.

4.3.4 Coexisting structures

As seen in figure 4.9, for the ^{192}Po and ^{194}Po isotopes the $J^{(1)}$ values derived from the $0^+_1 - 2^+_1$ energy difference are clearly smaller than the values extrapolated from the higher spin states. These irregularities can be due to crossing and mixing of two different coexisting structures. We have tested this interpretation by a simple two-level mixing calculation, similar to that performed by Oros et al. [Oro 99]. In these calculations the experimentally observed states are formed when close-lying pure spherical and deformed (oblate in this case) states with same spin and parity interact (see figure 4.11). As a result of the interaction the states get mixed and repel each other. The mixing amplitude b can be obtained from the formula [Oro 99]

$$\delta E = b^2 \Delta E_p, \tag{4.1}$$

where δE is the energy difference between the unperturbed and perturbed (experimental) states and ΔE_p the difference between the two perturbed states.

The low-spin level energies of the unperturbed oblate band in ^{192}Po and ^{194}Po are extrapolated from the experimental energies of the 4^+, 6^+, 8^+ and 10^+ levels, which are assumed to be unmixed members of the oblate band. Because the first excited 0^+ states (0^+_2) are not experimentally observed in ^{192}Po and ^{194}Po the values for the perturbed energies of these states were taken from the work of Oros et al. [Oro 99]. These values are obtained from the potential energy surface (PES) calculations which in heavier Po isotopes give 0^+_2 energies very close to the experimentally observed ones.

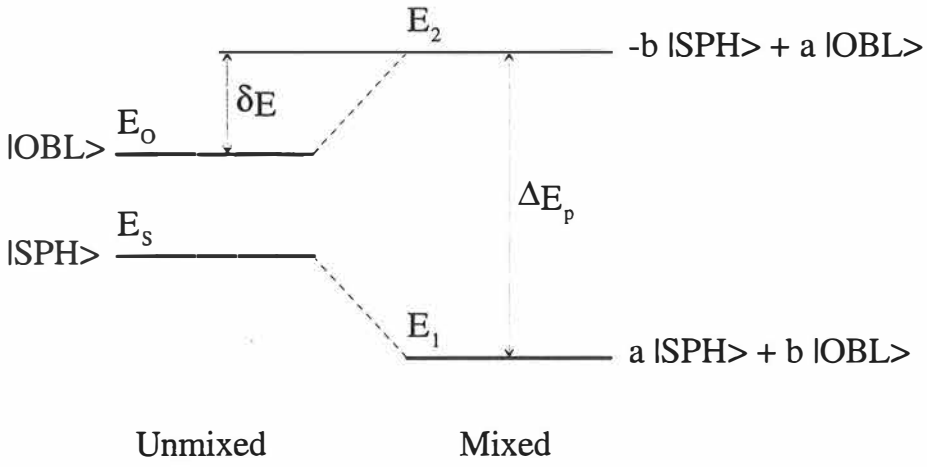

Figure 4.11. Schematic drawing of two-level mixing between the spherical (SPH) and oblate deformed (OBL) states.

Unperturbed level energies obtained from the mixing calculation are shown in figure 4.12. The energies are normalised to the experimental 0^+ ground state (0^+_1). It is interesting to see that the deformed bandhead 0^+ state, which in ^{194}Po is still slightly above the spherical one, has become the ground-state structure in ^{192}Po. In the experimentally observed levels the mixture of the deformed state in the 0^+ ground state increases from 45% in ^{194}Po to 73% in ^{192}Po. This change was also proposed by Allatt et al. on the basis of the α-decay studies [All 98], where the corresponding value of ~ 63% was derived for ^{192}Po. The observed 2^+_1 state of ^{194}Po is 99% of deformed structure. This value is calculated using our new 2^+_2 level energy. A similar value can be expected also for the 2^+_1 state in ^{192}Po by comparing the experimental 2^+_1 energy with the one extrapolated from the energies of the higher spin states.

It is interesting to note that the unperturbed spherical $0^+ - 2^+$ energy difference is very similar to the experimentally observed $0^+_1 - 2^+_1$ difference in the heavier polonium nuclei with A = 200 - 208. This is in accordance with the scheme of having the level structure of ^{194}Po as the spherical normal states crossed by the deformed intruder states. Using an empirical fit to the available data, the absolute value of deformation parameters β_2 can be estimated from the $2^+ \rightarrow 0^+$ transition energy [Gro 62]. In this

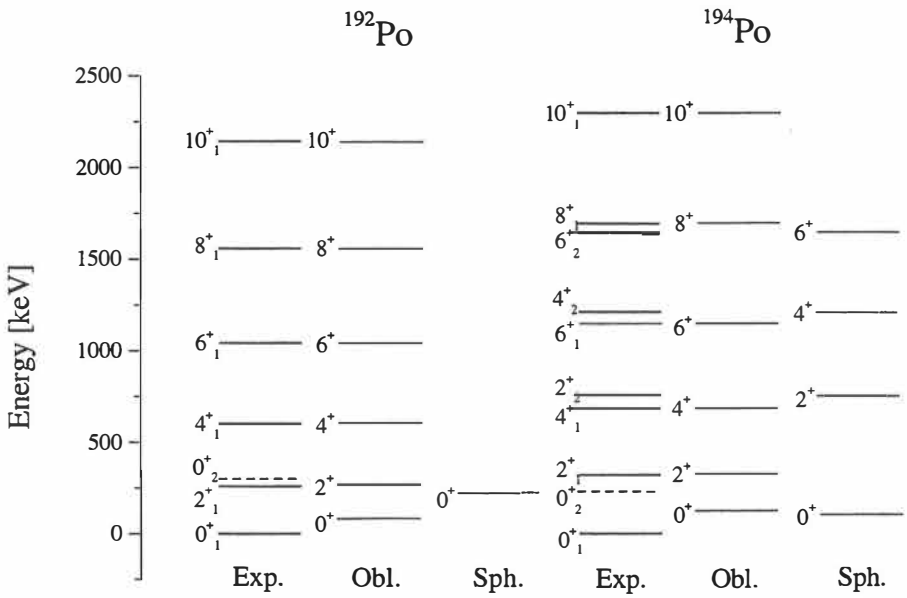

Figure 4.12. Experimental and unperturbed spherical and oblate deformed level energies for ^{192}Po and ^{194}Po. The energies are normalized with respect to the experimental 0^+_1 states.

way β_2 values for the unperturbed intruder bands in ^{194}Po and ^{192}Po can be estimated to be about 0.17 and 0.18, respectively. They are not far from the theoretically predicted [May 77], [Oro 99] oblate deformation parameters $|\beta_2| \approx 0.2$.

4.3.5. E0 transitions

Considerable E0 components in the $4^+_2 \rightarrow 4^+_1$ and $2^+_2 \rightarrow 2^+_1$ transitions of ^{198}Po have been reported by Alber et al. [Alb 91] on the basis of missing γ-ray intensities. This observation was used as an evidence to support the view of mixed coexisting structures of different shapes. However, in the more recent measurements Bernstein et al. [Ber 95] could not find any evidence for strong E0 components in the same transitions of ^{198}Po as well as of ^{196}Po. This result was used as an argument against the deformed intruder picture and to support the vibrational view. From our $\gamma\gamma$ coincidence data we have extracted, for the corresponding transitions in ^{194}Po, percentages of 38(20)% and 8(33)%, respectively, for the missing γ-ray intensities. In

the following we consider more closely the E0 transitions in ^{194}Po, ^{196}Po and ^{198}Po and their appearance as measurable E0 components.

In the simple coexistence model electric monopole transitions are allowed between spherical and deformed states of same spin and parity only if these states are mixed [Kan 79]. The monopole strength parameter ρ can be obtained from the formula [Kan 79], [Blo 78]

$$\rho \approx abk\beta_2^2, \tag{4.2}$$

where a and b are the mixing amplitudes, β_2 is the deformation parameter and

$$k = \frac{3}{4\pi} ZeR^2 \left[1 + \frac{4\pi^2}{3} \left(\frac{a_0}{R} \right)^2 \right], \tag{4.3}$$

where a_0 is the diffuseness parameter of the nuclear surface and R is the nuclear radius [Boh 75]. The low-energy E0 transitions proceed via internal conversion and the transition probability can be written as

$$\lambda(E0) = \rho^2 \sum_i \Omega_i, \tag{4.4}$$

where Ω_i is the energy-dependent electronic factor for i=K,L,... conversion [Bel 70]. The ρ^2 values for the $2^+_2 \rightarrow 2^+_1$ and $4^+_2 \rightarrow 4^+_1$ transitions in ^{194}Po, ^{196}Po and ^{198}Po were calculated by using the mixing amplitudes obtained from [Oro 99] and the present work. The deformation parameter $\beta_2 = -0.2$ predicted for the oblate structure both in [May 77] and [Oro 99] was used. The resulting ρ^2 values shown in table 4.6 demonstrate how the E0 rates can vary in the adjacent even-mass Po isotopes because of different mixing between the states involved. It should also be noted that the E0 transition rate is related to fourth power of the deformation parameter β_2. Consequently, the ρ^2 values given in table 4.6 would be reduced by factor of two if the deformation parameter β_2 would turn out to be −0.17 instead of −0.2.

The actual contribution of the E0 transitions in the observed intensities depends on the speed of the competing E2 or M1 γ–ray transitions. By using the ρ^2 values of table 4.6 and by assuming pure E2 character for the competing γ–ray transitions, estimates for the E0 contributions in the $2^+_2 \rightarrow 2^+_1$ and $4^+_2 \rightarrow 4^+_1$ transitions in ^{194}Po, ^{196}Po and ^{198}Po were derived. These estimates for the cases of the competing E2 rates being of 1, 10 and 100 Weisskopf units, are shown in table 4.7. In this table corresponding experimental E0 contributions obtained in the present work (^{194}Po) and derived from the data given in [Alb 91] (^{198}Po) and in [Ber 95] (^{196}Po, ^{198}Po) are also presented. This table together with the facts related to table 4.6 demonstrates how difficult it is, without information about the competing γ–ray transition rates, to draw any decisive conclusion about deformation for the states involved. It is interesting to note that, taking error bars into account, the E0 contributions in the transitions of ^{198}Po taken from the data of refs. [Alb 91] and [Ber 95] and shown in table 4.7 are consistent. Still the conclusions drawn from these results were contradictory.

Table 4.6. Calculated ρ^2 values for the $2^+_2 \rightarrow 2^+_1$ and $4^+_2 \rightarrow 4^+_1$ monopole transitions in ^{194,196,198}Po.

Nucleus	$\rho^2(2^+_2 \rightarrow 2^+_1)$ [10^{-3}]	$\rho^2(4^+_2 \rightarrow 4^+_1)$ [10^{-3}]
^{194}Po	10	0
^{196}Po	152	178
^{198}Po	28	173

Table 4.7. Estimated percentages of E0 transitions of all the transitions between equal spin states of ^{194,196,198}Po. The values are calculated for three different E2 strengths and compared with measured missing γ-ray intensity values ([Alb 91], [Ber 95] and this work).

Transitions	B(E2) = 1 W.u.	B(E2) = 10 W.u.	B(E2) = 100 W.u.	Meas. 1 [Alb 91]	Meas. 2 [Ber 95]	Meas. 3
^{194}Po($2^+_2 \rightarrow 2^+_1$)	75%	23%	3%			38(20)%
^{194}Po($4^+_2 \rightarrow 4^+_1$)	0%	0%	0%			8(33)%
^{196}Po($2^+_2 \rightarrow 2^+_1$)	99%	88%	42%		≤21%	
^{196}Po($4^+_2 \rightarrow 4^+_1$)	97%	75%	23%		≤55%	
^{198}Po($2^+_2 \rightarrow 2^+_1$)	89%	45%	8%	34(10)%	11(42)%	
^{198}Po($4^+_2 \rightarrow 4^+_1$)	99%	95%	64%	≥67%	49(29)%	

4.3.6 Isomeric states

In neutron deficient even-mass Po isotopes isomeric states with $I^{\pi} = 8^+$, 11^- and 12^+ have been found [Maj 86], [Maj 90], [Alb 91]. In the isotopes from ^{210}Po down to ^{198}Po the 8^+ isomer can be associated with the $\pi h_{9/2}^2$ multiplet. Due to the sudden drop of the energy of the yrast 6^+ state this 8^+ state is no longer isomeric in ^{196}Po.

Isomeric 12^+ states of the $\nu i_{13/2}^2$ configuration are observed in the even-A polonium isotopes from ^{202}Po to ^{198}Po [Maj 90].

The third observed isomer, with $I^{\pi} = 11^-$, has been found in all of the neutron deficient even-mass Po isotopes down to ^{196}Po. The g-factors measured for these states [Maj 90] reveal their dominant configuration of $\pi h_{9/2} i_{13/2}$. The B(E3) values for the $11^- \rightarrow 8^+$ transitions strongly increase with decreasing neutron number, reaching a value of 27(5) W.u. in ^{196}Po [Alb 91]. This is taken as an indication of the onset of collective E3 admixture in this transition and a possible appearance of a low-lying collective 3^- state. From our tentative result for the corresponding transition in ^{194}Po a B(E3) value of 7.9(15) W.u. was extracted. This value indicates weakening of the octupole collectivity compared to the heavier Po isotopes. However, the identification of the 459 keV $11^- \rightarrow 8^+$ transition was not firm. If the transition energy is calculated from the B(E3) value of ^{196}Po and the observed half-life in ^{194}Po, a value of about 54 keV is obtained. However, this energy is not reasonable when considering the energy level systematics. On the other hand, the existence of a 12^+ isomer possibly feeding the 11^- isomer cannot be ruled out. This feeding could increase the half-life measured for the 11^- state and thus result seemingly in the B(E3) value being smaller than expected.

The decay of the isomeric 11^- state in Po isotopes with N = 114 - 118, 124, 126 proceeds via the $\pi h_{9/2}^2$ 8^+ state. It could be expected that also in the more collective ^{194,196}Po nuclei the 11^- state would still de-excite to the 8^+ state with a dominant $\pi h_{9/2}^2$ configuration. Therefore the yrast 1939 keV 8^+ state in ^{196}Po and the non-yrast 2066 keV (8^+) state in ^{194}Po can be associated with the $\pi h_{9/2}^2$ configuration.

4.3.7 Odd-mass nuclei

In figure 4.13 energies of yrast levels of the even neutron deficient Po nuclei are compared with the level structure built on top of the isomeric $13/2^+$ state in the odd mass Po nuclei. It can be seen that especially in the lightest isotopes the level patterns of the odd mass nuclei are close to the ones of the adjacent even mass isotopes. This can be interpreted as a weak coupling of the odd $i_{13/2}$ neutron to the even-mass core. Here, due to the Coriolis force the nucleonic angular momentum j of the odd particle is aligned with the rotational angular momentum of the core and the nucleon can be considered as a spectator particle not affecting the structure of the core nucleus. This is typical for the nuclei having a weak deformation or small value of the projection of j on the deformation axis (Ω) in the deformed nuclei. If the deformation is large enough to split a single j state to different Ω states according to the Nilsson model the Coriolis interaction between the core and the odd nucleus decreases as Ω increases. Finally, with maximum Ω the angular momentum of the odd nucleon is aligned with the deformation axis and the nucleon is strongly coupled with the core. The strong coupling is experimentally observed as an appearance of a band consisting of strong mixed M1/E2 transitions between energy levels having a spin difference of $\Delta I = 1$ and weak E2 transitions between the $\Delta I = 2$ levels. Between the weak and strong coupling limits a number of transitional level structures exists. Typical for these is the appearance and lowering of the unfavoured spin levels, i.e. the levels with spin values differing by I = 1 with the levels seen in the weak coupling limit. The described coupling phenomena appear especially clearly in the nuclei where the odd nucleon is in a high-j unique parity state. This is the situation in the neutron deficient Po nuclei where the $i_{13/2}$ shell opens at neutron number $N < 114$. In ^{193}Po and ^{195}Po we have found candidates for the $15/2^+$, $19/2^+$ and $23/2^+$ states of the unfavoured $i_{13/2}$ band. In ^{193}Po the unfavoured states come down closer to the favoured ones indicating a change towards strong-coupling scheme when the number of neutron holes increases. This behavior is characteristic for an oblate deformed rotor since the Ω increases and thus the Coriolis force decreases when depleting the $i_{13/2}$ shell. Thus, the observation of a low-lying unfavoured spin band in $^{(195,)193}$Po is in agreement with the picture of the onset of oblate deformation at low spins in light Po nuclei with $N \approx 108$.

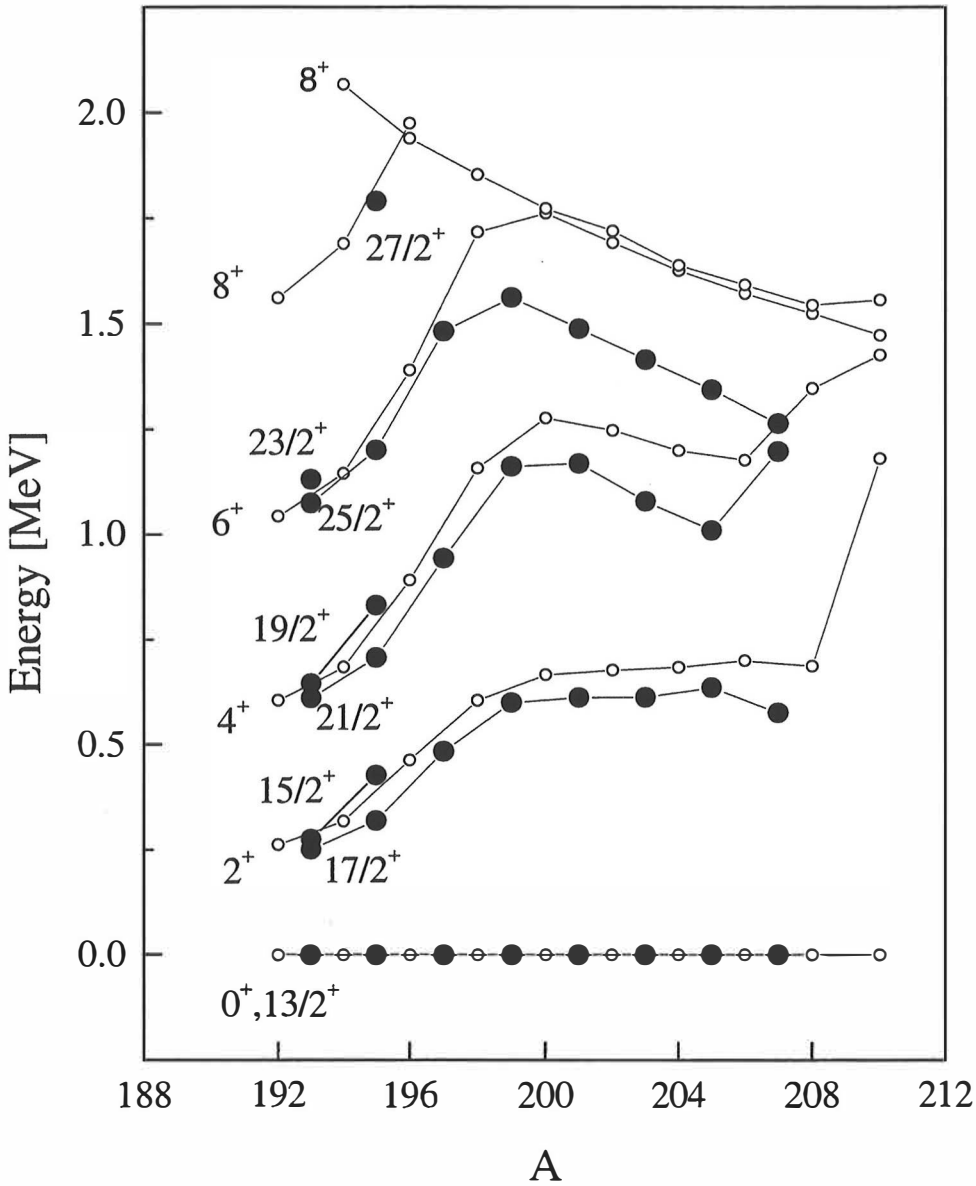

Figure 4.13. Energies of the yrast levels of the even-mass $^{192\text{-}210}$Po nuclei (open circles) together with the levels built on the top of the 13/2$^+$ states in the odd-mass $^{193\text{-}207}$Po nuclei (filled circles).

5. SUMMARY

The JYFL gas-filled recoil separator RITU has been combined with the Compton-suppressed Ge-detector arrays DORIS and Jurosphere for in-beam gamma-ray spectroscopic measurements. By employing recoil-decay tagging techniques it has been possible to extend γ-ray spectroscopic studies to very neutron deficient Po nuclei, produced at the few microbarn cross-section level.

In this work, comprehensive γ-ray spectroscopic studies of very neutron-deficient $^{192-195}$Po nuclei have been carried out by employing the recoil-decay tagging (RDT) and recoil gating methods for both prompt and delayed γ rays. The yrast line up to the (10^+) state in the ^{192}Po isotope, produced with a cross-section of only about 10 μb, was identified for the first time. The γγ-coincidence and angular-distribution information for ^{194}Po enabled the yrast states to be extended up to (16^+) and the identification of the second excited 2^+, 4^+, 6^+, (8^+) and (10) states as well as the negative parity 7^-, 9^- and isomeric (11^-) states. In the odd-mass isotopes ^{193}Po and ^{195}Po, yrast and nonyrast states on top of the $13/2^+$ state have been identified.

Our new data are in accordance with the picture of the coexisting normal spherical and intruding oblate states crossing each other when going to the Po isotopes with N < 114. The new data for ^{192}Po revealing signs of flattening of the level-energy systematics. This together with the simple mixing calculations show that the intruder structures have reached the ground state at N = 108 as predicted earlier in the Nilsson-Strutinsky type of calculations [May 77]. Comparison of the yrast-level energies of the light odd- and even-mass Po isotopes show that the $i_{13/2}$ neutron is weakly coupled to the even-mass core. The observed behavior of the unfavoured states can be explained by this coupling if the core has an oblate shape.

Many of the observed properties of light Po isotopes can also be described within the simple quadrupole vibrational model. Our view is that there is not necessarily any contradiction between the simple vibrational and the coexistence pictures. The situation is somewhat similar to that in the midshell Cd [Kum 90] and Te [Juu 99]

nuclei, where the proton intruder states clearly play a role in generating low-lying quadrupole phonon states.

Basic ideas and analysis methods related to the recoil gating and recoil-decay tagging techniques have been discussed in this thesis. This work formed the basis for the later use of the system in similar measurements: new γ-ray transition data on about 30 isotopes with no earlier information on the excited states have been collected. A new area of in-beam γ-ray spectroscopy, namely the heavy elements ^{254}No [Lei 99] and ^{252}No, have been reached.

REFERENCES

[Alb 91] D. Alber, R. Alfier, C.E. Bach, D.B. Fossan, H. Grawe, H. Kluge, M. Lach, K.H. Maier, M. Schramm, R. Schubart, M.P. Waring, L. Wood, H. Hübel, J. Zhang. Zeitschrift für Physik A 339 (1991) 225.

[All 98] R.G. Allatt, R.D. Page, M.Leino, T. Enqvist, K. Eskola, P.T. Greenlees, P. Jones, R. Julin, P. Kuusiniemi, W.H. Trzaska and J. Uusitalo. Physics Letters B 437 (1998) 29.

[And 99a] A. Andreyev, M. Huyse, P. Van Duppen, J.F.C. Cocks, K. Helariutta, H. Kettunen, P. Kuusiniemi, M. Leino, W.H. Trzaska, K. Eskola, R. Wyss. Physical Review Letters 82 (1999) 1819.

[And 99b] A. Andreyev et al. To be published.

[Ari 77] A. Arima, T. Ohtsuka, F. Iachello, I. Talmi. Physics Letters B 66 (1977) 205.

[Arm 71] P. Armbruster, J. Eidens, J.W. Grüter, H. Lawin, E. Roeckl and K. Sistemich. Nuclear Instruments and Methods 91 (1971) 499.

[Bar 91] B.R. Barrett, G.D. Dracoulis, R.A. Bark. Physical Review C 43 (1991) R926.

[Bax 93] A.M. Baxter, A.P. Byrne, G.D. Dracoulis, R.V.F. Janssens, I.G. Bearden, R.G. Henry, D. Nisius, C.N. Davids, T.L. Khoo, T. Lauritsen, H. Penttilä, D.J. Henderson, M.P. Carpenter. Physical Review C 48 (1993) R2140.

[Bea 92] C.W. Beausang, S.A. Forbes, P. Fallon, P.J. Nolan, P.J. Twin, J.N. Mo, J.C. Lisle, M.A. Bentley, J. Simpson, F.A. Beck, D. Curien, G. de France, G. Duchêne, D. Popescu. Nuclear Instruments and Methods in Physics Research A313 (1992) 37.

[Bel 70] D.A. Bell, C.E. Aveledo, M.G. Davidson, J.P. Davidson. Canadian Journal of Physics 48 (1970) 2542.

[Ber 95] L.A. Bernstein, J.A. Cizewski, H.-Q. Jin, W. Younes, R.G. Henry, L.P. Farris, A. Charos, M.P. Carpenter, R.V.F. Janssens, T.L. Khoo, T. Lauritsen, I.G. Bearden, D. Ye, J.A. Becker, E.A. Henry, M.J. Brinkman, J.R. Hughes, A. Kuhnert, T.F. Wang, M.A. Stoyer, R.M. Diamond, F.S. Stephens, M.A. Deleplanque, A.O. Macchiavelli, I.Y. Lee, B. Cedervall, J.R.B. Oliveira, J. Burde, P. Fallon, C. Duyar, J.E. Draper, E. Rubel, D.T. Vo. Physical Review C 52 (1995) 621.

[Bij 95] N. Bijnens, P. Decrock, S. Franchoo, M. Gaelens, M. Huyse, H.-Y. Hwang, I. Reusen, J. Szerypo, J. von Schwarzenberg, J. Wauters, J.G. Correia, A. Jokinen, P. Van Duppen, the ISOLDE collaboration. Physical Review Letters 75 (1995) 4571.

[Bij 96] N. Bijnens, I. Ahmad, A.N. Andreyev, J.C. Batchelder, C.R. Bingham, D. Blumenthal, B.C. Busse, X.S. Chen, L.F. Conticchio, C.N. Davids, M. Huyse, R.F.V. Janssens, P. Mantica, H. Penttilä, W. Reviol, D. Seweryniak, P. Van Duppen, W.B. Walters, J. Wauters, B.E. Zimmerman. Zeitschrift für Physik A 356 (1996) 3.

[Bij 98] N. Bijnens, P. Decrock, S. Franchoo, M. Gaelens, M. Huyse, H.-Y. Hwang, I. Reusen, J. Szerypo, J. von Schwarzenberg, G. Vancraeynest, P. Van Duppen, J. Wauters. Physical Review C 58 (1998) 754.

[Blo 78] J. Blomqvist. Private communication 1978.

[Blu 96] D.J. Blumenthal, C.N. Davids, C.J. Lister, D. Seweryniak, M.P. Carpenter, R.V.F. Janssens, D. Nisius, W. Gelletly, P. Regan, P. Woods, D.D. Warner, J. Simpson, S.J. Freeman, J. Schwartz, B. Field. Bulletin of The American Physical Society 41 (1996) 861.

[Boh 41] N. Bohr. Physical Review 59 (1941) 270.

[Boh 75] A. Bohr, B.R. Mottelson, Nuclear Structure, Vol. II, W.A. Benjamin Inc., Reading 1975.

[Ciz 98] J.A. Cizewski, K.Y. Ding, N. Fotiades, D.P. McNabb, W. Younes, R. Julin, J. Cocks, P. Greenlees, K. Helariutta, P. Jones, S. Juutinen, H. Kankaanpää, H. Kettunen, P. Kuusiniemi, M. Muikku, P. Rahkila, A. Savelius, C.N. Davids, R.V.F. Janssens, D. Seweryniak, M.P. Carpenter, H. Amro, P. Decrock, P. Reiter, D. Nisius, L.T. Brown, S. Fischer, T. Lauritsen, J. Wauters, C.R. Bingham, M. Huyse, A. Andreyev. Conference contribution, ENAM98: Exotic Nuclei and Atomic Masses.

[Coh 58] B.L. Cohen, C.B. Fulmer. Nuclear Physics 6 (1958) 547-560.

[Cre 91] J. Cresswell. Eurogam project documentation, document EDOC073, Nuclear structure software support group, Liverpool University, February 1991.

[Cul 98] D.M. Cullen, N. Amzal, A.J. Boston, P.A. Butler, A. Keenan, E.S. Paul, H.C. Scraggs, A.M. Bruce, C.M. Parry, J.F.C. Cocks, K. Helariutta, P.M. Jones, R. Julin, S. Juutinen, H. Kankaanpää, H. Kettunen, P. Kuusiniemi, M. Leino, M. Muikku, A. Savelius. Physical Review C 58 (1998) 846.

[Cur 98] P. Curie, M. Curie. Comptes Rendus 127 (1898) 175.

[Dav 92] C.N. Davids, B.B. Back, K. Bindra, D.J. Henderson, W. Kutschera, T. Lauritsen, Y. Nagame, P. Sugathan, A.V. Ramayya, W.B. Walters. Nuclear Instruments and Methods in Physics Research B70 (1992) 358.

[Dra 94] G.D. Dracoulis. Physical Review C 49 (1994) 3324.

[Dup 84] P. Van Duppen, E. Coenen, K. Deneffe, M. Huyse, K. Heyde, P. Van Isacker. Physical Review Letters 52 (1984) 1974.

[Fir 96] R.B Firestone, V.S. Shirley (editor), C.M. Baglin, S.Y. Frank Chu, J. Zipkin (assistant editors). Table of Isotopes, 8th ed. Vol. II, John Wiley & sons, Inc. 1996 New York.

[Fot 97a] N. Fotiades, W. Younes, J.A. Cizewski, D.P. McNabb, K.Y. Ding, C.N. Davids, R.V.F. Janssens, D. Seweryniak, M.P. Carpenter, H. Amro, P. Decrock, P. Reiter, D. Nisius, L.T. Brown, S. Fischer, T. Lauritsen, J. Wauters, C.R. Bingham, M. Huyse, A. Andreyev, L.F. Conticchio. Physical Review C 55 (1997) 1724.

[Fot 97b] N. Fotiades, J.A. Cizewski, D.P. McNabb, K.Y. Ding, C.N. Davids, R.V.F. Janssens, D. Seweryniak, M.P. Carpenter, H. Amro, P. Decrock, P. Reiter, D. Nisius, L.T. Brown, S. Fischer, T. Lauritsen, J. Wauters, C.R. Bingham, M. Huyse, A. Andreyev, L.F. Conticchio. Physical Review C 56 (1997) 723.

[Ghi 88] A. Ghiorso, S. Yashita, M.E. Leino, L. Frank, J. Kalnins, P. Ambruster, J.-P. Dufour, P.K. Lemmertz. Nuclear Instruments and Methods in Physics Research A269 (1988) 192-201.

[Gro 62] L. Grodzins, Physics Letters 2 (1962) 88.

[Hee 93] J. Heese, K.H. Maier, H. Grawe, H. Kluge, M. Schramm, R. Schubart, K. Spohr, W. Meczynski, M. Janicki, J. Styczen, J. Grebosz. Acta Physica Polonica B24 (1993) 61.

[Hel 96] K. Helariutta, T. Enqvist, P. Jones, R. Julin, S. Juutinen, P. Jämsen, H. Kankaanpää, P. Kuusiniemi, M. Leino, M. Muikku, M. Piiparinen, A. Savelius, W.H. Trzaska, S. Törmänen, J. Uusitalo, R.G. Allatt, P.A. Butler, P.T. Greenlees, R.D. Page. Physical Review C 54 (1996) R2799.

[Hel 99] K. Helariutta, J.F.C. Cocks, T. Enqvist, P.T. Greenlees, P. Jones, R. Julin, S. Juutinen, P. Jämsen, H. Kankaanpää, H. Kettunen, P. Kuusiniemi, M. Leino, M. Muikku, M. Piiparinen, P. Rahkila, A. Savelius, W.H. Trzaska, S. Törmänen, J. Uusitalo, R.G. Allatt, P.A. Butler, R.D. Page, M. Kapusta. To be published.

[Hey 92] K. Heyde, C. De Coster, J. Jolie, J.L. Wood. Physical Review C 46 (1992) 541.

[Jam 88] A.N. James, T.P. Morrison, K.L. Ying, K.A. Connell, H.G. Price, J. Simpson. Nuclear Instruments and Methods in Physics Research A267 (1988) 144.

[Joh 93] A. Johnson, D. Seweryniak, B. Cederwall, J. Nyberg, A. Atac, J. Blomqvist, J. Cederkäll, C. Fahlander, M. Karny, A. Kerek, J. Kownacki, L.-O. Norlin, R. Wyss, E. Adamides, H. Grawe, E. Ideguchi, R. Julin, S. Juutinen, W. Karczmarczyk, S. Mitarai, M. Piiparinen, R. Schubart, G. Sletten, S. Törmänen, A. Virtanen. Nuclear Physics A557 (1993) 401c.

[Jon 95] P.M. Jones. Ph.D. thesis, University of Liverpool, September 1995 (unpublished).

[Juu 99] S. Juutinen et al., to be published.

[Kan 79] J. Kantele, R. Julin, M. Luontama, A. Passoja, T. Poikolainen, A. Bäcklin, N.-G. Jonsson. Zeitschrift für Physik A 289 (1979) 157.

[Kan 95] J. Kantele, Handbook of Nuclear Spectrometry. Academic Press, 1995.

[Kum 90] J. Kumpulainen, R. Julin, J. Kantele, A. Passoja, W.H. Trzaska, E. Verho, J. Väärämäki. Zeitschrift für Physik A 335 (1990) 109.

[Lee 90] I-Y. Lee. Nuclear Physics A520 (1990) 641c.

[Lei 95a] M. Leino, J. Äystö, T. Enqvist, A. Jokinen, M. Nurmia, A. Ostrowski, W.H. Trzaska, J. Uusitalo, K. Eskola, P. Ambruster, V. Ninov. Acta Physica Polonica B26 (1995) 309.

[Lei 95b] M. Leino, J. Äystö, T. Enqvist, P. Heikkinen, A. Jokinen, M. Nurmia, A. Ostrowski, W.H. Trzaska, J. Uusitalo, K. Eskola, P. Ambruster, V. Ninov. Nuclear Instruments and Methods in Physics Research B99 (1995) 653.

[Lei 99] M. Leino, H. Kankaanpää, R.-D. Herzberg, A.J. Chewter, F.P. Heßberger, Y. Le Coz, F. Becker, P.A. Butler, J.F.C. Cocks, O.Dorvaux, K. Eskola, J. Gerl, P.T. Greenlees, K. Helariutta, M. Houry, G.D. Jones, P. Jones, R. Julin, S. Juutinen, H. Kettunen, T.L. Khoo, A. Kleinböhl, W. Korten, P. Kuusiniemi, R. Lucas, M. Muikku, P. Nieminen, R.D. Page, P. Rahkila, P. Reiter, A. Savelius, Ch. Schlegel, Ch. Theisen, W.H. Trzaska, H.-J. Wollersheim. To be published in European Physics Journal.

[Lis 87] C.J. Lister, M. Campbell, A.A. Chishti, W. Gelletly, L. Goettig, R. Moscrop, B.J. Varley, A.N. James, T. Morrison, H.G. Price, J.

Simpson, K. Connel, O. Skeppstedt. Physical Review Letters 59 (1987) 1270.

[Maj 86] A. Maj, H. Grawe, H. Kluge, A. Kuhnert, K.H. Maier, R.A. Meyer, J. Recht, N. Roy. Zeitschrift für Physik A 324 (1986) 123.

[Maj 90] A. Maj, H. Grawe, H. Kluge, A. Kuhnert, K.H. Maier, J. Recht, N. Roy, H. Hübel, M. Guttormsen. Nuclear Physics A 509 (1990) 413.

[May 77] F.R. May, V.V. Pashkevich, S. Frauendorf. Physics Letters B 68 (1977) 113.

[Mui 98] M. Muikku, J.F.C. Cocks, K. Helariutta, P.M. Jones, R. Julin, S. Juutinen, H. Kankaanpää, H. Kettunen, P. Kuusiniemi, M. Leino, P. Rahkila, A. Savelius, W. Trzaska, J. Uusitalo, P.T. Greenlees, R.D. Page. Physical Review C 58 (1998) R3033.

[Mün 79] G. Münzenberg, W. Faust, S. Hofmann, P. Armbruster, K. Güttner, H. Ewald. Nuclear Instruments and Methods 161 (1979) 65.

[Naz 93] W. Nazarewicz. Physics Letters B 305 (1993) 195.

[Nol 85] P.J. Nolan, D.W. Gifford, P.J. Twin. Nuclear Instruments and Methods in Physics Research A236 (1985) 95.

[Nol 86] P.J. Nolan. Proceedings of International Nuclear Physics Conference (Harrogate, UK, 1986), editors J.L. Durell et al. Bristol: IOP Conference Series 86, vol. 2.

[Oro 99] A.M. Oros, K. Heyde, C. de Coster, B. Decroix, R. Wyss, B. Barrett, P. Navratil. Nuclear Physics A 645 (1999) 107.

[Pau 95] E.S. Paul, P.J. Woods, T. Davinson, R.D. Page, P.J. Sellin, C.W. Beausang, R.M. Clark, R.A. Cunningham, S.A. Forbes, D.B. Fossan, A. Gizon, J. Gizon, K. Hauschild, I.M. Hibbert, A.N. James, D.R. LaFosse, I. Lazarus, H. Schnare, J. Simpson, R. Wadsworth, M.P. Waring. Physical Review C 51 (1995) 78.

[Rad 95] D.C. Radford. Nuclear Instruments and Methods in Physics Research A 361 (1995) 297.

[Sav 98] A. Savelius. Ph.D. Thesis, Department of Physics, University of Jyväskylä, Research Report No. 9/1998 (unpublished).

[Sch 79] K.-H. Schmidt, W. Faust, G. Münzenberg, H.-G. Clerc, W. Lang, K. Pielenz, D. Vermeulen, H. Wohlfarth, H. Ewald, K. Güttner. Nuclear Physics A318 (1979) 253.

[Sch 84] K.-H. Schmidt, C.-C. Sahm, K. Pielenz, H.-G. Clerc. Zeitschrift für Physik A 316 (1984) 19.

[Sim 86] R.S. Simon, K.-H. Schmidt, F.P. Heßberger, S. Hlavac, M. Honusek, G. Münzenberg, H.-G. Clerc, U. Gollerthan, W. Schwab. Zeitschrift für Physik A 325 (1986) 197.

[Sle 90] G. Sletten, J. Gascon, J. Nyberg. International Conference on Spectroscopy of Heavy Nuclei (Crete, Greece, 1989), International Physics Conference Series 105 (1990) 125.

[Spo 95] P. Spolaore, D. Ackermann, P. Bednarczyk, G. De Angelis, D. Napoli, C. Rossi Alvarez, D. Bazzacco, R. Burch, L. Müller, G.F. Segato, F. Scarlassara. Nuclear Instruments and Methods in Physics Research A 359 (1995) 500.

[Tay 99] R.B.E. Taylor, S.J. Freeman, J.L. Durell, M.J. Leddy, S.D. Robinson, B.J. Varley, J.F.C. Cocks, K. Helariutta, P. Jones, R. Julin, S. Juutinen, H. Kankaanpää, A. Kanto, H. Kettunen, P. Kuusiniemi, M. Leino, M. Muikku, P. Rahkila, A. Savelius, P.T. Greenlees. Physical Review C 59 (1999) 673

[Uus 96] J. Uusitalo. Ph.D. Thesis, Department of Physics, University of Jyväskylä, Research Report No. 4/1996 (unpublished).

[Wau 92] J. Wauters, P. Dendooven, M. Huyse, G. Reusen, P. Lievens, P. Van Duppen, the ISOLDE collaboration. Zeitschrift für Physik A 344 (1992) 29.

[Wau 93] J. Wauters, P. Dendooven, M. Huyse, G. Reusen, P. Van Duppen, P. Lievens, the ISOLDE collaboration. Physical Review C 47 (1993) 1447.

[Wau 94] J. Wauters, N. Bijnens, P. Dendooven, M. Huyse, Han Yull Hwang, G. Reusen, J. von Schwartzenberg, P. Van Duppen, R. Kirchner, E Roeckl, the ISOLDE collaboration. Physical Review Letters 72 (1994) 1329.

[Woo 92] J.L. Wood, K. Heyde, M. Huyse, P. Van Duppen. Physics Reports (Review Section of Physics Letters) 215 (1992) 101.

[You 95] W. Younes, J.A. Cizewski, H.-Q. Jin, L.A. Bernstein, D.P. McNabb, C.N. Davids, R.F.V. Janssens, T.L. Khoo, C.J. Lister, D.J. Blumenthal, M.P. Carpenter, D. Henderson, R.G. Henry, T. Lauritsen, D.T. Nisius, H.T. Penttilä, M.W. Drigert. Physical Review C 52 (1995) R1723.

[You 97] W. Younes, J.A. Cizewski. Physical Review C 55 (1997) 1218.